Charles University in Prague
Faculty of Mathematics and Physics

DIPLOMA THESIS

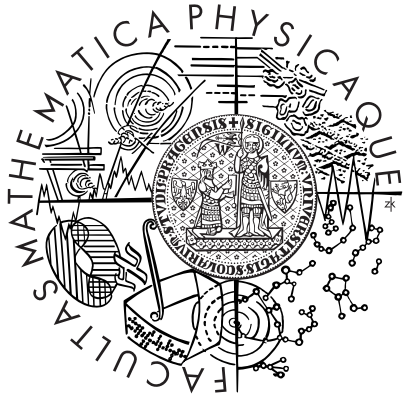

Marta Lungová

Structure and properties of nanophase separated hydrogels

Department of Macromolecular Physics

Supervisor: Doc. RNDr. Ivan Krakovský, CSc.

Study program: Physics of Condensed Matter

2010

Univerzita Karlova v Praze
Matematicko-fyzikální fakulta

DIPLOMOVÁ PRÁCE

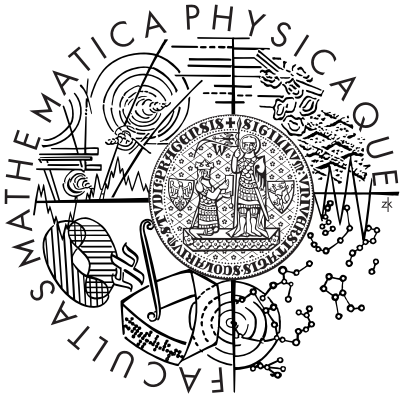

Marta Lungová

Struktura a vlastnosti nanofázově separovaných hydrogelů

Katedra makromolekulární fyziky

Vedoucí diplomové práce: Doc. RNDr. Ivan Krakovský, CSc.

Studijní program: Fyzika kondenzovaných soustav a materiálů

2010

I would like to express my gratitude to my supervisor, doc. Ivan Krakovský for his valuable help and supervision of my work. Many thanks also go to dr. Helena Valentová and dr. Ján Šomvársky from the Department of Macromolecular Physics for their valuable advices to special topics of polymer networks. I am indebted to prof. Manuel Monleon Pradas and his group in Centro de Biomateriales, Universidad Politécnica de Valencia for their assistance and advices in my experimental work perfomed in Valencia. My sincere appreciation goes to Ing. Miroslava Novotná (Institute of Chemical Technology, Prague) for her appreciable help with interpretation of infrared spectra.

Furthemore, I wish to thank ERASMUS programme for finacial support of my stay in Valencia. Financial support of EU in performing small-angle neutron scattering experiments discussed in this thesis in Budapest Neutron Centre (Contract No. RII3-CT-2003-505925) is also gratefully acknowledged.

This is to certify that this thesis has been composed by myself and that the references cited include all the sources of information I have utilized. I agree with lending this thesis.

Prohlašuji, že jsem svou diplomovou práci napsala samostatně a výhradně s použitím citovaných pramenů. Souhlasím se zapůjčováním práce.

Prague, 13th April 2010 Marta Lungová

Contents

Title of thesis: Structure and properties of nanophase separated hydrogels
Author: Marta Lungová
Department: Department of Macromolecular Physics
Supervisor: Doc. RNDr. Ivan Krakovský, CSc.
Contact: ivank@kmf.troja.mff.cuni.cz

Abstract: A central goal of this work is study of structure and mechanical and thermal properties of hydrogels prepared by swelling of hydrophilic polymer networks in water. To this purpose series of epoxy networks was prepared by reaction of α,ω-diamino terminated poly(oxypropylene)-*b*-poly(oxyethylene)-*b*-poly(oxypropylene)- with aromatic diepoxide (Bisphenol A propoxylate diglycidyl ether). Network formation process was monitored by Fourier transform infrared spectroscopy (FTIR) and gel permeation chromatography (GPC). Nanophase separation in the networks prepared has not been found by dynamic mechanical analysis (DMA) or differential scanning calorimetry (DSC). On the other hand, nanophase separated structure of the hydrogels has been revealed by small-angle neutron scattering (SANS). SANS data were fitted well using Teubner-Strey model based on the locally lamellar structure of water-rich and water-poor nanodomains and values of model parameters are determined. Formation of nanophase separated structure is attributed to high difference in the interaction of network components with water. Influence of water on thermal transitions in hydrogels is studied by DSC.

Keywords: nanophase separation, polymer hydrogels, epoxy networks

Název práce: Struktura a vlastnosti nanofázově separovaných hydrogelů
Autor: Marta Lungová
Katedra (ústav): Katedra makromolekulární fyziky
Vedoucí bakalářské práce: Doc. RNDr. Ivan Krakovský, CSc.
e-mail vedoucího: ivank@kmf.troja.mff.cuni.cz

Abstrakt: Hlavním cílem této práce je studium struktury a vlastností hydrogelů připravených botnáním hydrofilních polymerních sítí ve vodě. Pro tento účel byla pomocí reakce α,ω- diamino končeného poly(oxypropylen)-*b*-poly(oxyethylen)-*b*-poly-(oxypropylen)u s aromatickýcm diepoxidem (propoxylát diglycidyléteru Bisphenolu A) připravena série epoxidových sítí. Proces tvorby sítě byl sledován kombinací inračervené spektroskopie s Fourierovou transformací (FTIR) a gelové permeační chromatografie (GPC). Dynamická mechanická analýza (DMA) ani diferenční skanovací kalorimetrie (DSC) nepotvrdily, že by v sítích došlo k nanofázové separaci. Naproti tomu, u hydrogelů byla pomocí maloúhlového rozptylu neutronů (SANS) nanofázově separovaná struktura prokázána. SANS experimentální data byly úspěšně fitovány použitím Teubner-Streyova modelu, který je založen na lokálně lamelární struktuře nanodomén s vysokým nebo nízkým obsahem vody a byly stanoveny parametry modelu. Příčinou vzniku nanofázově separované struktury je velký rozdíl v interakci složek sítě s vodou. Vliv vody na termické přechody v hydrogelech je studován pomocí DSC.

Klíčová slova: nanofázová separace, polymerní hydrogely, epoxidové sítě

0.1 List of Symbols and Abbreviations

b_{i}	coherent scattering length of the nucleus
b_{coh}	coherent neutron scattering lengths
b_{inc}	incoherent neutron scattering lengths
c_p	molar heat capacity at constant pressure
c_{NH2}	molar concentration of amine groups in ED600
c_{E}	molar concentration of epoxy groups in PDGEBA
d	specific mass
d_{p}	specific mass of dry extracted network
d_{s}	specific mass of solvent
f	frequency
k	Boltzmann constant
k_{spring}	power constant of spring
m	mass of hydrogel
m_{p}	mass of dry extracted network
m_1	mass of point 1
m_2	mass of point 2
q	scattering vector
q_{max}	value of scattering vector in a maximum of intensity
r	initial molar ratio of amine hydrogens to epoxy groups $= 2\ [\mathrm{NH_2}]_0/[\mathrm{E}]_0$
v_{p}	volume fraction of polymer
v_{s}	volume fraction of solvent
v_{H2O}	volume fraction of $\mathrm{H_2O}$
w	mass fraction of one component in two-component system
w_{g}	mass fractions of gel
w_{s}	mass fractions of sol
w_{PDGEBA}	mass fractions of diepoxide
w_{POE}	mass fractions of poly(oxyethylene)
w_{POP}	mass fractions of poly(oxypropylene)
x	parameter in equation for structure factor $= 2qR_H$
X	ratio of polymer to solvent molar volume
D	periodicity of locally lamellar structure
D_{B}	Bragg distance
E'	storage (elastic) modulus – real part of absolute dynamical modulus
E''	loss modulus – imaginary part of absolute dynamical modulus
E_{aff}	theoretical Young modulus for affine model
E_{dyn}	elastic modulus of non-extracted networks obtained by dynamical experiment at 0.1 Hz and 20 °C

E_{exp}	experimental modulus obtained by DMA
E_{hgel}	Young modulus of non-extracted hydrogel determined from stress-strain curves at 20 °C
E_{netw}	Young modulus of non-extracted network determined from stress-strain curves at 20 °C
E_{ph}	theoretical Young modulus for phantom model
E_{red}	reduced Young modulus
$E_{\mathrm{red}}^{\mathrm{aff}}$	reduced Young modulus of affine network
$E_{\mathrm{red}}^{\mathrm{ph}}$	reduced Young modulus of phantom network
E_{n}	quantised oscillator energy
[E]	concentration of epoxy groups
$[\mathrm{E}]_0$	initial concentration of epoxy groups
G	Gibbs free energy
G_{el}	elastic Gibbs free energy
I	scattering intensity
I_{B}	incoherent scattering intensity (background)
I_{L}	contribution from dynamic inhomogeneities to intensity
I_{SL}	contribution from frozen inhomogeneities to intensity
L	length of the specimen
L_0	initial length of the specimen
M_{c}	average molar mass of elastically active network chains
M_1	average molar mass of ED600 taken from producer
M_{OP}	molar mass of oxypropylene unit
M_{osm}	osmotic modulus
M_2	average molar mass of PDGEBA taken from producer
N	number of atoms
N_p	number of polymer segments
N_s	number of solvent molecules
$[\mathrm{NH_2}]_0$	initial concentration of amine groups
Q	scattering invariant $= 2\pi^2\langle(\Delta\varrho)^2\rangle$
R	universal gas constant
R_{H}	minimus distance between scattering bodies in Percus-Yevick model
T	absolute temperature
T_α	glass transition temperature obtained by dynamical experiment
T_{a}	temperature determined from thermogram that speak about transition steepness
T_{b}	temperature determined from thermogram that speak about transition steepness
T_{g}	glass transition temperature
T_1	temperature where the tangent of heat flow leaves the experimental curve below T_{g}
T_2	temperature where the tangent of heat flow leaves the experimental curve above T_{g}
Z	atomic number

Δc_p	change of molar heat capacity at constant pressure
ΔH_c	enthalpy of crystallization
ΔH_m	enthalpy of melting
ϵ	strain $= (L - L_0)/L_0$
$\hbar$	Planck constant
χ	polymer to solvent interaction parameter
λ	stretching ratio in uniaxial extension $= L/L_0$
$\lambda_x, \lambda_y, \lambda_z,$	stretching ratios in x, y, z-direction
λ_n	wavelength of neutron
μ	reduced mass
μ_p	chemical potential of polymer
μ_s	chemical potential of solvent
μ_a	numbers of elastically active junctions
ν	characteristic vibration frequency
ν_a	numbers of elastically active chains
$\tilde{\nu}$	quantity referred to wavenumber
$\langle(\Delta\varrho)^2\rangle$	mean square density fluctuation of the scattering length density
ω	frequency of oscillator vibrations
ϱ_A	neutron scattering length density of phase A
ϱ_B	neutron scattering length density of phase B
ϱ_p	neutron scattering length density of polymer
ϱ_s	neutron scattering length density of solvent
ρ	measure of the strength of substitution effect
$\tan\delta$	loss factor (phase shift) $= E''/E'$
θ	scattering angle
ξ	cycle rank
ξ_L	correlation lengths of polymer gel
Ξ	characteristic lengths of frozen inhomogeneities
ζ	persistent length of lamellar order

DMA	Dynamic mechanical analysis
DMSO	dimethyl sulphoxide
DSC	Differential scanning calorimetry
EANC	elasticaly active network chain
FTIR	Fourier transform infrared spectroscopy
FTIR-ATR	Fourier transform infrared – Atenuated total reflectance spectroscopy
GPC	Gell permeation chromatography
PDGEBA	bisphenol A diglycidyl ether propoxylate
POE	poly(oxyethylene)
POP	poly(oxypropylene)
SANS	Small-angle neutron scattering
SAXS	Small-angle X-ray scattering

Chapter 1

Introduction

The present work is dedicated to hydrophilic epoxy networks prepared by reaction of a diamine based on telechelic polyoxypropylene-*b*-polyoxyethylene-*b*-polyoxypropylene (POP-*b*-POE-*b*-POP) with an aromatic diepoxide and to hydrogels prepared from them. Hydrophilic epoxy networks belong to a broad class of epoxy resins with modified properties. Copolymers of POE are widely used in biomedical applications since POE is inert to human body.

Previous works [1], [2], [3] deal with similar systems including longer POE and POP blocks which led to a nanophase separation in the networks of ratio of functional group higher than 1.25. The type of a phase structure was investigated using SANS resulting in conclusion about water-rich phase of water and POE segments and water-poor phase of PDGEBA and POP segments. Therefore a similar phase separation was also expected for our samples with shorter segments. In addition, there is a question if the segments will form the same arrangements in the case of short lengths.

For the better insight into the networks structure they were proceeded as extracted and non-extracted samples, dried, partially and fully swollen in water, methanol and other solvents. Thus the hydrophilicity of POE segments in contrast to hydrophobicity of POP segments can be heightened and allowed us to study phase separation by the methods used in this work. Finally, the possible substitution effect on amine groups, which was an object of interest in more foregoing works, was studied.

Variety of methods used for structure analysis offered better understanding of influence of more aspects to chains arrangements. Dynamical mechanical analysis (DMA) is frequently applied for finding macroscopical mechanical properties that reflect microscopical parameters. An important phenomenon of glass transition can be observed by DMA. This process occurs in dependence on experimental setup and differentiation of network segments. However, Differential scanning calorimetry (DSC) seems to be much better method for studying of phase separation inside the networks. By this method crystallization and a melting point can be studied. Because an additional ingredient to liquid can shift its melting or crystallization temperature, DSC measurement is able to give information about the type of phase separation and mixing of possible segments. For detailed analysis based on microstructure focus the Small-angle neutron scattering (SANS) was chosen. Herein a possibility of

evaluation of Bragg distance together with the other structure parameters from scattering pattern presents a big advantage of this method. In addition, fitting of resulting diagram helps with the description of a type of phase separation. Finally, the substitution effect on amine groups as the possible aspect of influencing the polymerization was studied using Gel permeation chromatography (GPC) and Attenuated total reflectance (ATR – FTIR). The effect, in a case of marked power, should cause a production of long linear oligomers at the beginning of reaction that would connect to 3D network just after one reaction of the most of amine groups is determined. As a result, the structure of non-stoichiometry network would differ. Missing of non-linear oligomers in polymer mixture detected by GPC can prove an importance of substitution effect in our systems. After polymerization, conversion of functional groups of monomers was studied by ATR – FTIR.

Conception of the thesis is composed of six chapters. Introduction to issue of studied polymers, theory using in interpretation of experiments and description of methods builds a framework of theoretical part in chapter 3. Experimental part is presented into chapter 4 with specification of experimental work in laboratory, results and discussion together with comparison of resultant values with the expected from the theory in chapter 5 and global conclusion in the last chapter 6.

1.1 Polymeric hydrogels

Definition of hydrogels describes them as 3D junctioned solid systems swollen in water to high degree. Today we know natural or synthetic hydrogels that contain over 99 % of water. Hydrogels possess valuable flexibility due to their significant water content, but no fluidity. This characteristic designates them as appropriate for tissue engineering for their distinct similarity to natural tissue. A typical hydrogel is situated in a medusa body, shellfish, in plants or in a human body. Hydrogels often exhibit density closed to a density of water.

The most popular and important application of hydrogel is in medicine and tissue engineering. The appropriate solvent of monomers can be transported to an injured organ, here the solution polymerizes in accordance with a specific body need and free volume and substitutes a part of injured organ. Another widely used utilization of medical hydrogels as biocompatible implants lies in surgically inserting of ready-made hydrogel to a body instead of diseased organ. After some time body cells expand to hydrogel cavities and with substantially degradation of hydrogel skeleton the organ can be repaired by body own matter. For implants the materials such as hyaluronan, agarose or methylcellulose are frequently used.

Hydrogel can react to changes of pH, temperature and other surround conditions and through the process of collapse it can be used as medicament delivery system. Relatively high absorption and debriding capacity of hydrogel is utilized in medical dressing. Usually we can meet hydrogel plasters.

Hydrogels that are responsive to some specific molecules, such as glucose or antigens, can be used as biosensors.

Contact lenses comprise a big part of utilization of hydrogels. Their contemporary composition was invented by the Czech professor Otto Wichterle in the Institute of

Macromolecular Chemistry in Prague. He supplanted hard and rigid lenses by those from hydrogels that are more compatible and comfortable for human eye.

Hydrogels with weak connections are produced by a lot of companies as cosmetic substances, e.g. hair fixation gel, massage gel, etc.

Among the novelties a special textile structure of so-called hydrojacket has been designed to give more comfort and safety to the Fireman's activities.

At home the hydrogel pellets for plants are seen even more frequently. These pellets have considerable absorption ability and after swollen they hold constant wet in vase or in container with a plant.

In addition, everybody knows such hydrogel as jelly of various colours which is so fine and tasty on cake.

1.2 Thermodynamics of phase separation and swelling

Phase separation is a thermodynamical process by which a system is separated into two or more phases of different composition and properties. It is dependent on Gibbs phase rule that talks about the relation between a number of components c, number of independent intensive variables (or degree of freedom) f and possible phases p that can exist in equilibrium:

$$c + 2 = f + p \tag{1.1}$$

Phase can be described as a region of material that is chemically uniform, physically distinct, and (often) mechanically separable. Typical phases are solid, liquid and gas, however chemistry deals with a lot of other phases, as an example the regions with higher and lower degree of swollen form two different phases.

Phase separation became favourite phenomenon in last decades in connection with nanoscale materials. Scientists have found big potential in using this process for production of various materials with scale under 100 nm.

Equilibrium of a thermodynamic system at constant pressure and temperature corresponds to a minimum of Gibbs free energy. With an aim to find a theoretical expression for the Gibbs free energy of a polymer solution or blend lattice models are used. Mean field approach is used in Flory - Huggins theory which provides the expression for G as

$$G = N_\mathrm{s}\mu_\mathrm{s}^0 + N_\mathrm{p}\mu_\mathrm{p}^0 + kT[(N_\mathrm{s} + \mathrm{X}N_\mathrm{p})\chi v_\mathrm{s}v_\mathrm{p} + N_\mathrm{s}\ln v_\mathrm{s} + N_\mathrm{p}\ln v_\mathrm{p}] \tag{1.2}$$

where N_s, N_p are the numbers of solvent molecules and polymer segments, μ_s^0 and μ_p^0 are the chemical potentials of neat solvent and polymer, k is Boltzmann constant, T is the absolute temperature, v_s and v_p are volume fractions of solvent and polymer, X is the ratio of polymer to solvent molar volume and χ is the polymer-solvent interaction parameter. The first term in brackets describes mixing enthalpy, the second and third one mixing entropy. The last part of 1.2 represents mixing Gibbs free energy.

In addition, process of swelling is accompanied by a network expansion, therefore, an elastic contribution to changes of Gibbs free energy. For isotropic expansion of the three-dimensional polymer network upon swelling it accounts:

$$G_{\mathrm{el}} = \frac{3}{2} E(\lambda^2 - 1) \tag{1.3}$$

where E is the Young elastic modulus, λ is the stretching (or linear swelling) ratio.

Both increments depend on more conditions. Nevertheless, during swelling the constant temperature and pressure and unchanging number of polymeric elements can be considered in the system. For swelling process the progress of Gibbs free energy should be expressed as dependent on swelling degree, which is identical to ν_s, using a sum of mixing and elastic increment (see Fig. 1.2). The elastic increment increases mainly by higher swelling degree together with internal stress between junctions. For explanation, elastically active chains are extended with solvent absorption, thus their elasticity potential decreases. Oppositely, the mixing increment decreases with higher v_{s} which is caused and influenced mostly by interaction parameter. With higher swelling degree of the ratio of elements in contact with those other component becomes lower. Definitely, the total increment of G assumes one minimum at possible swelling degree which means the equilibrium value.

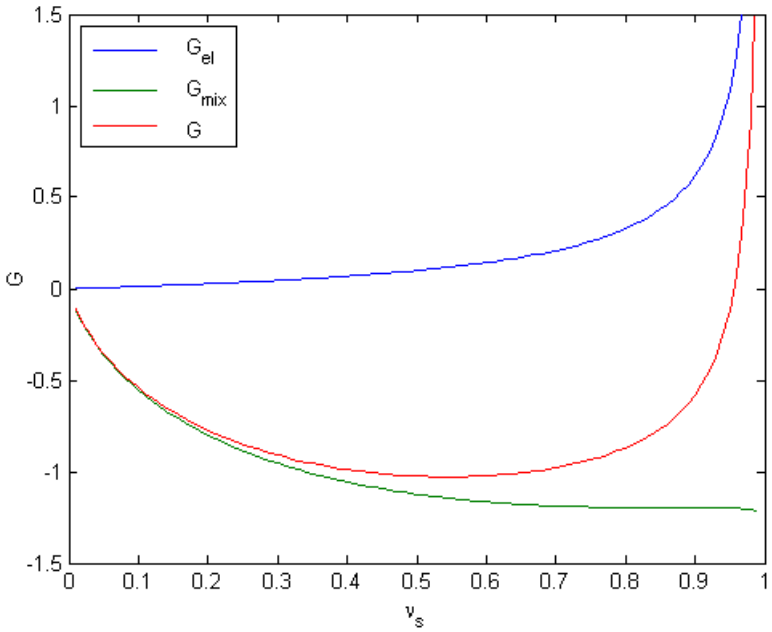

Figure 1.1: An example of theoretical change of Gibbs free energy during swelling. The green curve represents mixing increment, the blue means elastic increment and the red curve is sum of both.

1.3 Production of nanomaterials

A prefix 'nano' seems to be one of the most popular word among the scientists in the recent years. Many of them foresee a big potential of nanomaterials for life in future. Therefore, many innovation methods for production of materials structured at nanometer length scale have been developed. Among them the often employed are

- *Grinding* is one of top down method by which additive pellets are used and resulting material can reach diameter about 5 nm.
- *Rolling* is similar method as preceding, but produced layers are free of additive material and of size ca 50 nm.
- *Cutting* with diamond enable sheet of size less than 100 nm.
- *Electrospinning* is industrially appropriate way how to generate large volume of nanofibres more rapidly. It is based on electrostatic forces between charged cylinder periodically wetted to monomer solution and inversely charged electrode on which the fibres are collected.
- *Drawing* from small drop is only laboratory technology with more disadvantages such as low speed, larger diameter of fibre.
- *Template synthesis* from special materials (metal oxides), monomer solution is pulled through the template filled by pores of defined sizes.
- *Self – assembly* allows a production of very thin nanofibres, but the diameter and length are hardly controllable. This bottom-up method bases on attractive forces between similar fragments, so the micellar structures appear in the solution.
- *Chemical vapor deposition* means deposition of the most metal vapor on surface. This is used for surface treatment.
- *Phase separation* serves as an agreeable technique for material with nanoscale pores or cavities. This is one of bottom-up methods with high advantage of wide choice of chemical compositions and possibility to control structure of material by reaction conditions.
- *Molecular beam epitaxy* requires temperature above 750 °C, etc.

The reason, why we have chosen phase separation rely on simplicity of its realization, possibility of making substances of various sizes, chemical structure and physical properties.

Two-phase matter can be realized for example by the addition of solvent monomer solution that is excluded to free volume among macromolecule fragments during polymerization which causes origin of pores. Their diameters are dependent on more conditions such as solvent to monomer ratio, type and rate of polymerization, etc. Another method leading to nanomaterial inheres is using of elute-able nanocrystals.

These become part of macromolecule because they are immured among its walls. Appropriate solvent enables subsequent elution of the nanocrystals, the result is material with nanoscale pores. On the other side, the origin of small cavities and pores in the product can be an undesirable effect that often happens by too fast polycondensation. Our samples were prepared on the basis of different polarity and hydrophilicity of monomer segments which led to phase separation. The nanoscale structure was expected through phase separation to hydrophobic and hydrophilic phases. Intermolecular cohesive forces put the segments of similar properties together on the basis of cohesive energy. Existence of secondary cohesive bonds is a consequence of antisymmetricaly lay-out of positive and negative charge in molecules. Although the molecule behaves externally as neutral, the segments of opposite charges come close to each other. Small polarization which comes from movement of electrons, produce the attractive forces. The molecules with permanent dipoles exhibit higher cohesive forces. Permanent dipoles have a tendency to orientation according to external field, but this orientation can be disturbed by thermal movement. Hydrogen bonds represent the strongest types of secondary bonds. Usually they act as very important forces in hydrogels.[4]

1.4 Polymeric Networks

1.4.1 Epoxy resins

Epoxy resins cover a broad class of industrially popular substances with a wide variety of utilization. They provide one of the best adhesives known. They cause many different materials to adhere to each other by acting as a mutual bond between them. All the materials that can interact physically or chemically with the epoxy functional group can be glued by them. A mixture of epoxy resins and sand is frequently used in building industry in factory floors because of their resistivity from bases and acids or in areas where constant braking of trucks or automobiles would otherwise destroy the pavement. [5]

Because many materials exhibit good ability to adhering to epoxy resins, the utilization in area of coating is of the same importance. Epoxy surface coatings belong to the most widely used industrial finishes and provide superior adhesion, flexibility and corrosion resistance when applied to metallic substrates. Utilization of epoxy resins based on bisphenol A diglycidyl ether lies in protective coatings, including paints, in reinforced plastic laminates and composites, in tooling, casting and moulding resins, encapsulating, in bonding materials and adhesives, and in floorings and aggregates. Due to convenient mechanical properties, epoxy resins have found their place also in area of fiber-reinforced composites. [6]

The epoxy resins made their first debut by old sources around 1947 in the United States, where the first product on the basic of epoxy resins was produced by the Devoe-Reynolds Company. It was a polyalcohol for preparation of synthetic drying oils. After the Second World War the importance of resins began to grow. It was used in production of coatings. Later, the application of this substance extended to much more areas of industry. [7]

One advantage of epoxy resins lies in ability of polymerization without secondary

condensation products that could lead to porosity. In addition, they show low volume change during annealing which decreases internal tension. Epoxy resins are resistant to most of chemicals. They can be transparent or dark, flexible or rigid, slowly or fast polymerizable, etc.

Applications of epoxy resins cover wide spectrum of products:

- glue – fast polymerization, initiator is water so the surface of broken object must be free of oil.
- castings – parts of machine, toys, packaging.., less contraction than polyester resins, better chemical resistance, water resistance, combustibility is decreased by special additives such as MgO, Al_2O_3
- coatings – slow polymerization, monomer with initiator is absorbed to treated artefact and polymerize inside with the aim to improve its properties, this is mostly used in buildings, floors, wood. Additional advantage of using epoxy coatings is smooth surface
- trinket – is prepared as castings, too. Big advantage is a good price of products and big variety of colour and shape offering

The capital consumer of epoxy resins is China, just after this country is Western Europe and the third is the USA. The primary producers of monomers for the resins or of epoxy resins are Dow, Huntsman and Hexion.

1.4.2 Composition of epoxy resins

Epoxy resins consist of epoxy and hardener. As the epoxy monomer for example tetraglycidyl methylene dianiline – TGMDA, diglycidylether of bisphenol A – DGEBA, epoxyphenol cresol novolac or cycloaliphatic epoxies CA are used. Choice from wide offer depends on requirements of resulting product. Epoxies form the most important part of resins, however also the choice of hardener serves to extend the variability of epoxy resins. Aliphatic, aromatic amines, acid anhydrides and alcohols belong to the most utilized hardeners for epoxy resins. The flexibility or absorption ability of resins can be influenced by length of hardener molecules, those with double junction or aromatic substituent are more rigid.

Typically epoxy resins are prepared by the reaction of diamino-functionalized prepolymer (eventually diol or triol) with a diepoxide, e.g. α, ω – diamino terminated polyoxypropylene (POP) with diglycidyl ether of Bisphenol A (DGEBA), during which the initially liquid reaction mixture passes through a gel-point and solidifies into the polymer network. By using α, ω – diamino terminated POE hydrophilic networks can be prepared, however, high reactivity of amino groups in this case can cause a disadvantage in some applications. Therefore the other monomer α, ω – diamino terminated poly(oxypropylene)- block - poly(oxyethylene)- block - poly(oxypropylene) with higher molecular weight can be used because of its less reactivity. Hydrophobic parts represented by poly(oxypropylene) (POP) blocks bring in a special structure parameter. The epoxy networks prepared in this way have more attractive characteristics for biomedical applications. [8]

Block copolymers based exclusively on the hydrophilic POE and hydrophobic POP segments are broadly used in industry, pharmacy and cosmetics or e.g. as wetting agents, de-emulsifiers in oil recovery and detergents. Many works have been done as an examination of their stability during pH or temperature changes. The most of these works have an aim to improve current medical materials or pills, product latter with intelligent characteristics which would behave in accordance with surroundings. This is a way to production of such tablets that would begin their degradation in sick organ. Simultaneously the undesirable impacts of tables would be put down.

1.4.3 Inhomogeneity in epoxy systems

A variety of experiments deal with inhomogeneity of such systems even if they are prepared in stoichiometry. Some of the off-stochiometric epoxy-amine networks with very low crosslinking density exhibited a more clearly expressed structure than some highly crosslinked systems [9]. The reason for inhomogeneous structure of networks should be searched first of all in the reaction kinetics itself or, what is more relevant here, in the distribution of groups in various reaction states at conversions higher than zero. Specifically, for a diepoxide-diamine system with negligible substitution effect between epoxy and amino groups it means that the numbers of primary, secondary and tertiary amino groups should be the same as in a system consisting of monoepoxide-monoamine molecules at the same conversion. Such behaviour was proved up to and slightly beyond the gel point in really systems. If regions existed in the stoichiometric system richer in one or the other component, the crosslinking density of both regions would be lower than that expected for system in stoichiometry.

The tendency to inhomogeneous course of curing of epoxy resins and formation of inhomogeneously junctioned products can be attributed by more factors:

- **thermodynamic instability** or segregation developed during curing in systems consisting of partly compatible components
- simultaneously occurring **reactions producing domains** of chemically different units, which by itself can result into inhomogeneous crosslinking or can additionally induce physical segregation
- **extensive cyclization** which becomes important mainly in the homopolymerization.

The formation of cycles or elastically inactive cycles (loops) beyond the gel point, always accompanies branching and its intensity is dependent moreover on the reaction mechanism as well as on chain flexibility. On the other hand, the epoxy curing reactions are usually step reactions or slow polyaddition reactions with lower tendency to cyclization. However, cyclization can play a non-negligible role. Some monomers, such as PDGEBA in the reaction with diamines, exhibit a very low tendency to cyclization so that the ring-free theory, applied for network modeling, can be used successively. This conclusion was done on the basis of experiment by which

the critical conversion at the gel point was provided as independent on dilution for PDGEBA-diamine systems and because the critical conversion corresponds to the ring- free model. [9]

1.4.4 Reaction between epoxy and amine groups – principle of epoxy curing

The principle of step-wise polymerization in our system is well known among chemists. Its principle is sketched in Fig. 1.2. The diamine's electrons attack the carbon atom of epoxy group, giving a negative charge on the epoxy oxygen, and a positive charge on the nitrogen. A new bond is formed between the carbon and the amine nitrogen. The extra electron pair of oxygen takes a hydrogen from the ammonium nitrogen, making an alcohol group and an amine group.

Similarly, the leftover hydrogen from amine group can be removed by another bond with epoxide and the same on the opposite end of diamine molecule. So there four 'ways to infinity' from diamine and two ways from diepoxide can appear. The Fig. 1.3 shows a substructure of an ideal stoichiometric network. If amount of epoxy groups is lower than that of half of diamine groups, the non-stoichiometric networks are formed, where some amines have to be unbound or bound in only one junction. In the first case a dangling chain occurs in network, in the second case the chain of higher molecular weight is created between elastic active junctions.

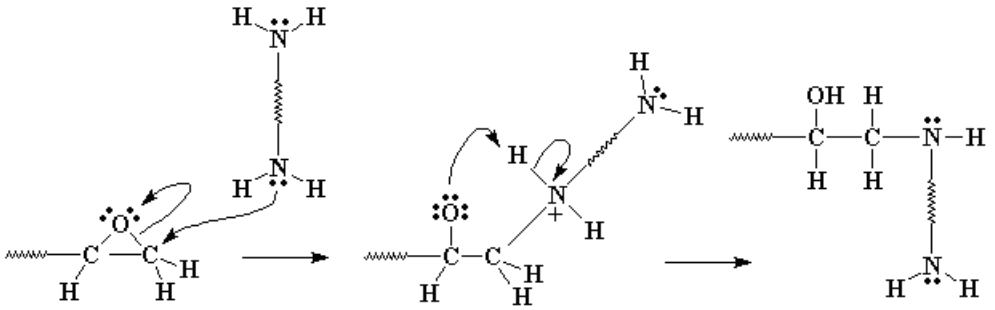

Figure 1.2: Scheme of reaction between epoxy and amine group. Reproduced from Ref. [10]

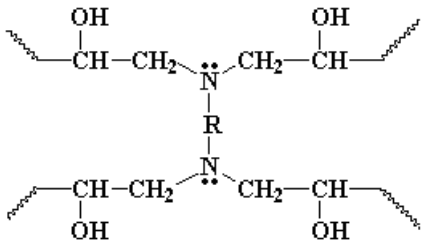

Figure 1.3: Substructure of an ideal stoichiometric network. Reproduced from Ref. [10]

The curing rate can be controlled through the chemical reactivity of monomers used for polymerization and other conditions. Theoretically, structure and characteristic of product is related to output from chemical kinetic equations and theory of branching processes. With respect to kinetic theory, the reaction rate is not controlled neither by diffusion of reacting species nor by segmental mobility at temperature above T_g. If the polymerization is controlled by simultaneous concentration of the activated complex consisted from more monomers connected together or by the diffusion constants of the species carrying the reactive groups, is contingent on reactive constants of both processes. Too low diffusion can contribute to higher degree of inhomogeneity and lower conversion. The rate of diffusion decreases rapidly with grow of activated segments in system. Therefore, during curing of some epoxy – curing agent systems the reaction is initially controlled by chemical reactivity of functional groups, but because T_g increases together with decreasing of mobility with conversion, the reaction rate becomes eventually controlled by overall diffusion. [11]

Regarding on foregoing works, it is legitimate to use the statistical approach. There only one type of bond origin in the system.

Substitution effect

The substitution effect in reaction of diepoxid and diamine determines whether extensive branching has already occurred in the early stages of curing, or whether chain extension predominates. The diepoxide PDGEBA seems to have the same and independent reactivity of both epoxy groups which was established in numbered works. Substitution effect in reactions of monoamines and polyamines with epoxides was investigated by many researchers. In polyamines, two substitution effects occur. One relates to the change of reactivity of one amine group induced by the reaction of another amine group, the other one concerns the activity of hydrogens in primary amine compared to that in the formed secondary amine. Typically, the substitution effect within the amine groups is caused by steric and electronic effects.

1.4.5 POE – POP – POE block copolymer

Copolymers are synthesized by polymerization of a mixture of two and more monomers (copolymerization). In copolymers properties of all monomers are combined. If monomers are built into copolymer chains in blocks a block copolymer is obtained. As a famous example of the block copolymer, polystyrene –*b*-polybutadiene-*b*-polystyrene (SBS) can be mentioned. For their production a living polymerization is used. At the first phase, the segments by desirable molar weight from one monomer are prepared. The termination of reaction is controlled by reaction conditions. Later on, another monomer is added to segments with the purpose of making second block. This procedure can be repeated with next monomer. Finely the two - or more – block copolymers can be connected by some hardener or trough reaction of edge functional groups.

Molecule of POE – POP – POE block copolymer consists of biocompatible blocks of relatively simple structure and preparation, POE block is highly hydrophilic and as a block copolymer exhibits thermoresponsive behaviour. It is a subject of great interest in many research works. For this copolymer a distinct leap of viscosity is

typical at set temperature (and concentration), denoted as lower critical solubility temperature - LCST. Two types of thermoresponsive behaviour of polymers are known, reverse thermal behaviour (RTB) and thermal degradation. It can be realized by gelation or transition 'coil to globule' which causes jump of viscosity. The first one is bound with rapid increasing of viscosity with temperature and has found application in tissue engineering. Monomer solution of lower viscosity is injected to injured organ and polymerizes at the required place so as the shape and size would be appropriate for body. With the second one, thermal degradation, everybody has already met in tablets. Their covering is made from thermal degradable polymer initializing the degradation when suitable conditions – temperature and pH of stomach or other parts of digestion system are reached. Choice of special polymer with fixed critical temperature or pH enables controlled releasing of medicament. Thermoresponsive behaviour is displayed by polymers with partially hydrophilic and partially hydrophobic character. Among such polymers the POE – POP – POE three-block similarly as poly(ethylene glycol)-poly(lactic acid)-poly(ethylene glycol) denoted as PEG-PLA-PEG belong to more important. They have been investigated for drug solubilization and controlled release, for the prevention of post – surgical tissue adhesions and in wound covering as RTB-displaying polymers [12]. Regrettably, the increase of viscosity achieved by these three-blocks was not large enough, stability was too small and polymers displayed short residence times and unacceptably high permeability. With the aim to improve mechanical properties, three-block has been connected by several hardeners, such as diisocyanates, phosgene and diacyl chlorides [13], length of three-block segments has been varied [1], [3], networks have been prepared from many different multiblock copolymers [12], etc. Each experiment was conditioned by requirements so variability of them results to variability of examined and generated systems.

1.5 Principles of experimental methods used

To analyze the networks more experimental methods were used. Following sections offer an introduction to principle of each method used to interpret the polymer structure.

1.5.1 GPC

Gel permeation chromatography (GPC) is essential in polymer chemistry to measure the distribution of molar masses. It is based on the ability of molecules to move through a gel column that has pores of clearly-defined sizes. The principle of measurement is elution of studied components with mobile phase through the stationary phase which is special gel for GPC. The larger molecules can not enter the pores so they pass quickly through the column and get out first. Smaller molecules can enter some pores and they elute later. The chronological succession of components is inversely proportional to their size and, thus, molecular weight. Principle of GPC is shown in Fig. 1.4. After elution from stationary phase the components are distinguished by detector. In GPC two types of detectors are often used. The first type is sensitive to concentration of components and includes UV absorption, differential refractometer or refractive index detectors, infrared absorption and density detector. The other type of detectors is represented by molecular weight sensitive detectors, such as low angle or multi angle light scattering detector. For this work, the refractive index detector was used.

The great advantage of the technique is its simplicity and rapid elution of large molecules. The method can be used to determine molecular weight of large biomolecules or polymers, as well as to separate them from salts and small molecules.

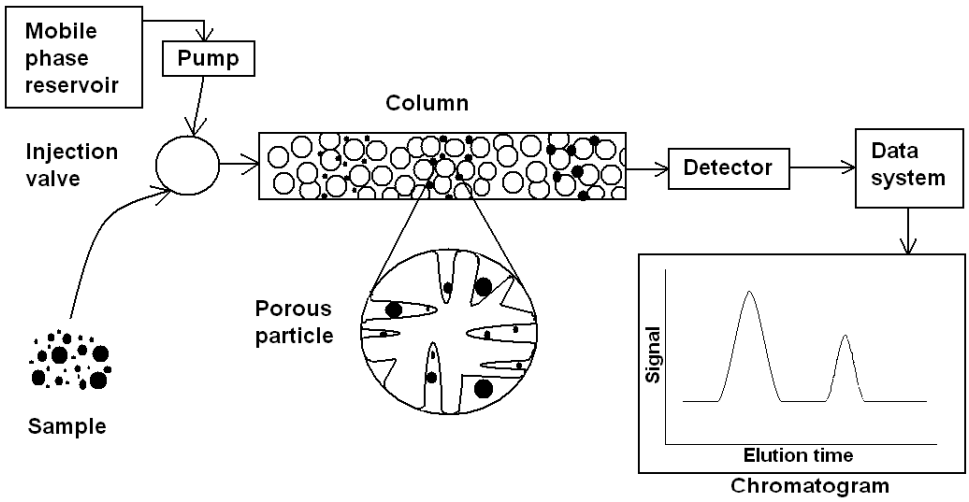

Figure 1.4: A lay-out of a GPC chromatograph. Mixture of sample and eluent is injected to column filled by porous particles. As the molecules traverse the column, the components of the sample are sieved based on differential pore permeation. Afterwards, detector is used for interpretation of fractions. Reproduced from Ref. [14]

1.5.2 FTIR

Fourier Transform Infrared Spectroscopy (FTIR), is a useful analysis technique that provides information about the chemical bonding or molecular structure of materials. It is mainly used in qualitative analysis to identify unknown materials presented in a specimen.

Principle of vibration spectroscopy

Molecules of substances around us are in permanent movement. A free molecule consisting of N atoms moves in:

1. translation which has 3 degrees of freedom,
2. rotation which has 3 or 2 degrees of freedom (2 refers to linear molecules),
3. vibration which has remaining $3N$-3 ($3N$-2) degrees of freedom.

Molecule vibration is primarily compared to harmonic oscillation of two mass points linked by a spring. Let masses of points are m_1, m_2 the spring is described by its power constant, k_{spring}, in molecular language the strength of atomic binding. Classical mechanics provides an equation for a vibration frequency ω of the spring:

$$\omega = \sqrt{\frac{k_{\text{spring}}}{\mu}} = 2\pi c\tilde{\nu} \qquad \mu = \frac{m_1 m_2}{m_1 + m_2} \tag{1.4}$$

where μ is the reduced mass of molecule, c is speed of light in vacuum and $\tilde{\nu}$ represents a quantity often used in vibration spectroscopy referred to as wavenumbers. This model is very useful since it enables a simple explanation of many important characteristics of vibration spectra. Heavy atoms will vibrate at lower frequencies, whereby those with higher power constant (which means stronger bonding) will vibrate at higher frequencies. This is the main principle of vibration spectroscopy to which infrared spectroscopy belongs.

In quantum mechanics, vibrating diatomic molecule is represented by one-dimensional quantum harmonic oscillator. Solution of the Schrödinger equation for this system leads to quantization of the oscillator energy by expression

$$E_n = \hbar\omega(n + 1/2) \tag{1.5}$$

where $\hbar$ is Planck constant, and n represents a positive integer. Therefore, the vibrating molecule can occupy various discrete energy levels, and moves to higher (lower) energy level after absorption (emission) of energy quantum.

Vibration spectrum is usually expressed as dependence of the absorbance, A, on wavenumbers, $\tilde{\nu}$. Absorption bands (peaks) are observed at wavenumbers corresponding to vibration transitions of the molecule. These frequencies are often characteristic for smaller groups of atoms in the molecule.

ATR-FTIR technique

Attenuated total reflection (ATR) is nowadays one of the most used FTIR techniques. It offers more advantages, for example simple sample preparation is required, absence of solvent which could influence resulting spectra, possibility to study strongly absorbing samples, solids, polymers, etc. Typical for ATR measurements is a very low depth of the infrared (IR) beam penetration into the sample. The infrared spectrum choice for vibrational spectroscopy is based on a low fluorescence probability. The process of analysis is quite simple, polymer sample of any thickness is placed onto the ATR crystal, and the pressure applied generates a nearly perfect result. The IR beam is directed into a crystal of a higher refractive index, so that the total reflection condition in the crystal is fulfilled if the sample refractive index is low enough and beam reflects in higher angle than the critical one. In the place of reflection on boundary between crystal and sample an evanescent wave origins and projects orthogonally into the sample in intimate contact with the ATR crystal. Some of the energy of evanescent wave is absorbed by the sample and the reflected radiation (thus partly absorbed by the sample) is returned to the detector, so that the absorbance can be measured. A simple scheme of ATR device is displayed in Fig. 1.5 with detail of evanescent wave originating in a sample. After absorption the beam is directed to the interferometer. The Fourier transformation of interferogram leads to final absorption spectrum.

For our samples ATR method was chosen because of its simplicity and because an ATR device is at our disposal in laboratory. All the analysed samples were dried, so the spectra were almost free of water peaks that is important for amine peaks observation around 3300 – 3400 cm^{-1}.

Corrections before and during experiment

Only a measurement that is done precisely can lead to acceptable results useful for further analysis and comparisons.To achieve this, several conditions must be met. Before the experiment a baseline should be measured without a sample. This gives background level that should be subtracted from the measured spectrum of sample. The baseline measurement enables to eliminate undesirable water peaks, carbon dioxide or other absorbing molecules from the sample environment. However, the substances concentration oscillates with time, so in the end the spectrum will display only small signs of contamination.

The best way of elimination the unwanted peaks is to repeat an experiment in multi-scan mode and subsequently to count all the scans. Assuming that fluctuations of impurities concentration are random, we can expect averaging of their peaks after few counted experiments. On the other side, one should be sure that the sample under study does not change during the experiment.

Contribution of vibration spectroscopy

Generally, vibration spectroscopy offers lot of information about chemical composition of a sample. In particular, spectroscopy helps analyzing individual groups binding, phase separation, unreacted functional groups, tacticity, etc. Besides the

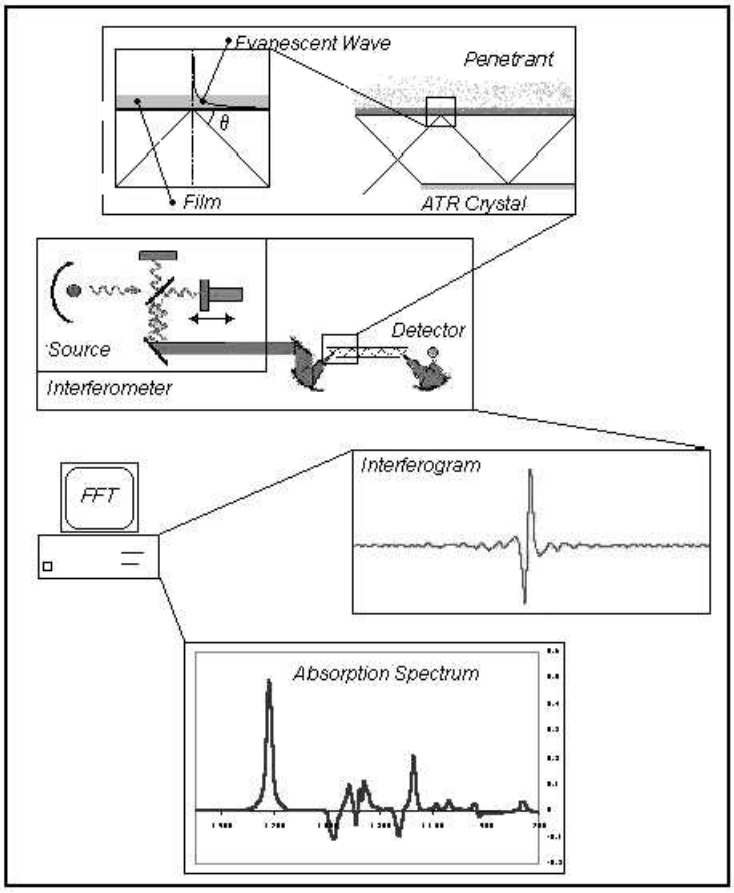

Figure 1.5: Principle of FTIR - ATR. Reproduced from Ref. [15]

qualitative analysis, it is possible to obtain also quantitative information, such as function groups or components ratio, water amount inside the sample, etc by comparison with some standard sample.

However, it is impossible to deduct the structure and composition of absolutely unknown material using only vibrational spectroscopy. For that additional information about the sample is required. Spectroscopy for elucidation of unknowns task should be considered as only auxiliary method.

1.5.3 SANS

Small-angle neutron scattering is one of the scattering methods that use a neutron beam as a source. In this technique thermalised neutrons with wavelength (1 - 10 Å) are scattered by a sample and the resulting scattering pattern contains an information about the structure of the sample on length scale 1 - 100 nm. In SANS of non-magnetic materials, neutrons are scattered by atomic nuclei which can be treated as point scatterers unlike small-angle X-ray radiation (SAXS) where photons are scattered by all electrons and their space distribution has to be considered (in atomic form factor). Neutron scattering power is measured by scattering lengths of nuclei, whereas X-ray scattering power by atomic number. Both, SANS and SAXS are not

sensitive to structural details on atomic length scale, but on larger scale, therefore they reflect fluctuations in neutron scattering length density and electron density, respectively. Contributions of light atoms, as hydrogen, to SAXS patterns are very weak unlike SANS (see Table 1.1). A big difference in neutron scattering properties of proton and deuterium

Atom	Z	b_{coh} [10^{-12} cm]	b_{inc} [10^{-12} cm]
H	1	-0.374	2.52
D	1	0.667	0.40
C	6	0.665	0.01
N	7	0.936	0.20
O	8	0.580	0.00

Table 1.1: Neutron scattering parameters of some atoms: Z is the atomic (proton) number, b_{coh} and b_{inc} are the coherent and incoherent neutron scattering lengths, respectively.

For wide area observations it is necessary to have good resolution at small angles, so the distance between sample and target is usually much longer in WANS/WAXS (Wide angle neutron/x-ray scattering).

Detailed SANS device description and theory is beyond the scope of this work, therefore only a short description is presented. The schematic experiment layout is given in Fig. 1.6. A neutron beam is produced by the horizontal cold source in the reactor. A wavelength selection is realized through a mechanical velocity selector consisting of a rotating drum with helically curved absorbing slits at its surface. Subsequently the beam enters the collimator which is composed of more waveguides. Unlike electromagnetic radiation (light or x-ray), neutrons cannot be easily focused. At the end of the collimation, the beam size in front of the sample is fixed by an aperture. The scattered neutrons are collected by a adjustable detector. By combining its distances from sample and the entire range of wavelengths, the total accessible scattering vector range is markedly increased. A detector rotation around its middle axis is also possible and useful at small distances from sample (less than 2 m) to correct from geometric distortions. [16]

SANS pattern expected from polymer solutions and gels

The SANS results are presented by means of scattering intensity I as a function of the magnitude of scattering vector, q. Scattering vector is the subtraction of wavevectors of scattered and beam neutrons and in case of elastic scattering its magnitude can be expressed by virtue of neutron wavelength, λ_{n} and scattering angle, θ by

$$q = \frac{4\pi}{\lambda_{\mathrm{n}}} \sin \frac{\theta}{2}. \tag{1.6}$$

In polymer networks swollen in a good solvent two types of concentration fluctuations are reflected in scattering patterns - dynamic fluctuations due to thermal movement of solvent molecules and polymer segments, and, frozen fluctuations

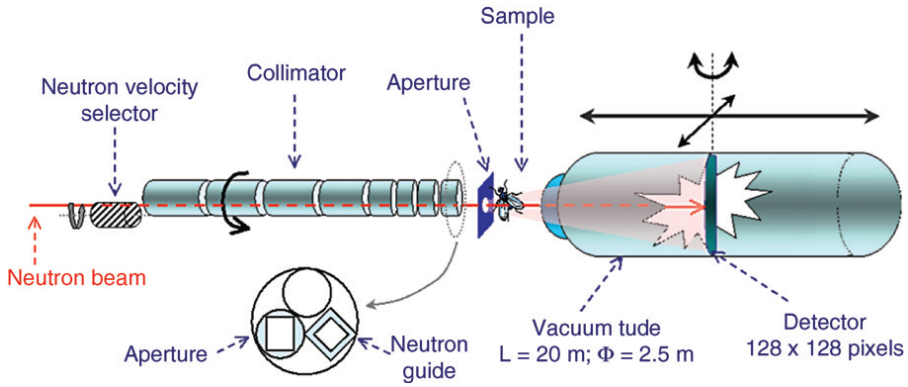

Figure 1.6: Schematic layout of the instrument for SANS experiment. Reproduced from Ref. [16]

due to inhomoegenous distribution of polymer network junctions, respectively. They make two terms in scattering intensity:

$$I(q) = (\varrho_{\mathrm{p}} - \varrho_{\mathrm{s}})^2 \left[\frac{A}{(1 + \Xi^2 q^2)^2} + \frac{kTv_{\mathrm{p}}^2}{M_{\mathrm{osm}}} \frac{1}{1 + \xi_{\mathrm{L}}^2 q^2} \right] + I_{\mathrm{B}} \tag{1.7}$$

where ϱ_{p} and ϱ_{s} are scattering lengths of polymer and solvent, respectively, A is a constant, Ξ is the characteristic length of frozen inhomogeneities and ξ_{L} is a correlation length of dynamic inhomogeneities and M_{osm} is the osmotic modulus. The presence of Ξ is characteristic feature of gels inhomogeneous space distribution of network junctions. Frozen inhomogeneities dominate on larger length scales than dynamic ones, therefore Ξ is much larger than ξ_{L} and their contribution is apparent in low q-region. I_{B} denotes the incoherent scattering intensity (background). [17]

To analyse the structure of samples investigated in this work, a proper model of nanophase separated structure allowing calculation of scattering intensity analogous to eg.1.7 is necessary. Various models have been proposed for different compositions of micro and nanophase separated copolymers [18]. Copolymers with more-less the same content of both components oriented to extensive parallel sheets can be described by an ideal lamellar model. However, this model does not appear to be a good candidate for interpretation of the scattering from rubber polymers. An idea of globular domains on a distorted lattice forms a concept of a Zernike-Prins model with constrained application only for crystal imperfections and other systems where the scattering bodies adopt a distorted lattice. A Percus-Yevick model considering globular domains in a liquid-like dispersion has been relatively successful in describing the scattering from microemulsions and some microphase-separated copolymers. To explain the broad scattering peak exhibited by microemulsions a periodic, random two-phase (Teubner-Strey) model was proposed which was successively used also for our systems.

The Percus-Yevick model suggests that the scattering observed from dense, disordered systems such as a liquid should be related to the Fourier transform of a pair correlation function $g(r)$ as a function of the positions of scatterers. Thus the

scattering intensity can be expressed as

$$I(q) = I_0 P(q) \left[1 - \langle n \rangle \int_0^\infty r^2 (g(r) - 1) \frac{\sin qr}{qr} dr\right] = I_0 P(q) S(q) \tag{1.8}$$

$$P(q) = 9(\Delta\rho)^2 v^2 \left[\frac{\sin(qR) - qR\cos(qR)}{(qR)^3}\right]^2 \tag{1.9}$$

where $\langle n \rangle$ is the average number density of scattering bodies, R and v is the radius and volume of spherical scattering bodies, respectively, $(\Delta\rho)^2$ is the square of the difference in electron density of alternating phases. The function $P(q)$ is the particle scattering factor observable from an isolated body in the absence of interference effects and $S(q)$ is the structure factor which depends on relative positions of neighbouring phases:

$$S(q) = \left[1 + \frac{24w}{x} G(x)\right]^{-1} \tag{1.10}$$

where $x = 2qR_{\mathrm{H}}$ and R_{H} is radius of the scattering body. Expression for $G(x)$ is complicated and the reader is referred to Ref. [18] for details.

This model assumes uniformity of spherical particles and equality of particle and interaction radii. It was successfully used for fitting the scattering of similar systems but with longer diamines which are arranged to separated spherulites of one phase dispersed in a matrix of the other phase. [19].

Another model was designed by Teubner and Strey [18]. The model origins from phenomenological Landau-Ginzburg theory of phase transitions and has been proved successful in fitting scattering data from microemulsions as well as polymer systems [20]. Unlike the Percus-Yevick model, in Teubner-Strey model the nanophase separated structure is not particular but locally lamellar. Two parameters, periodicity D, and persistent length of the locally lamellar order, ζ, are used. The scattering intensity is given by

$$I(q) = \frac{8\pi \langle (\Delta\varrho)^2 \rangle}{\zeta} \frac{1}{a_2 + c_1 q^2 + c_2 q^4} \tag{1.11}$$

where $\langle (\Delta\varrho)^2 \rangle$ is the mean square fluctuation of the scattering length density and a_2, c_1, c_2 are the coefficients originating from the expansion of system free energy in terms of order parameter and its derivatives. This function behaves like q^{-4} at high q- region. Two characteristic parameters of Teubner-Strey model can be expressed using the coefficients a_2, c_1, c_2 as

$$D = 2\pi \left[\frac{1}{2}\left(\frac{a_2}{c_2}\right)^{1/2} - \frac{1}{4}\frac{c_1}{c_2}\right]^{-1/2} \qquad \zeta = \left[\frac{1}{2}\left(\frac{a_2}{c_2}\right)^{1/2} + \frac{1}{4}\frac{c_1}{c_2}\right]^{-1/2} \tag{1.12}$$

1.5.4 DMA

Dynamic mechanical analysis is one of techniques of thermal analysis. In DMA a force is applied to sample and response of the material (strain) is measured. From DMA experiment we can determine viscoelastic properties of materials like storage and loss modulus. These are meassures of material ability to lose energy as a heat and to recover from the deformation. In dynamic regime, two different modes of operation are used: either periodical force with frequency f is applied to the sample, and amplitude and phase shift of strain are registered or vice versa. The two modes are referred to as stress and strain control, respectively. There are also a few deformation geometries used in DMA, e.g., uniaxial extension, three-point bending, simple shear, etc. In Fig. 1.7 one can see uniaxial extension mode which was also used in this work.

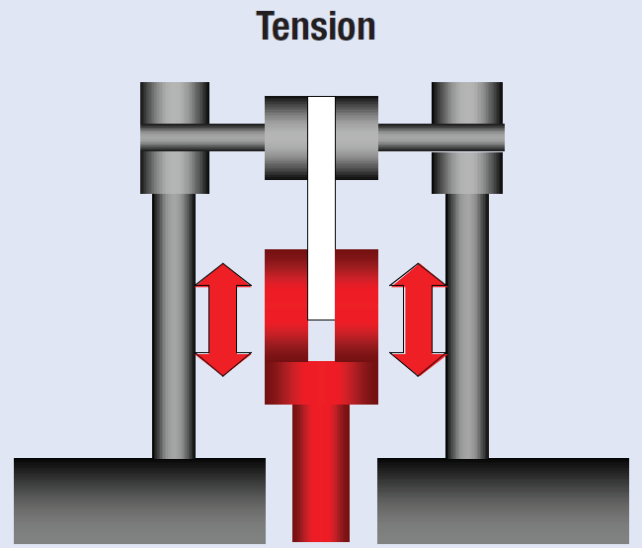

Figure 1.7: Uniaxial extension mode - sample is anchored on one end by a fixed clamp and by the drive shaft on the other. Tension stress is applied by the motor. Reproduced from Ref. [21]

In dynamic regime and small deformations, the stress-strain relation for isotropic materials (Hooke's law) is written in phasor notation (detailed deduction in [22]):

- absolute dynamical modulus

$$E^* = \frac{\sigma^*}{\varepsilon^*} \tag{1.13}$$

- real part of modulus – elastic modulus or modulus in phase

$$E' = \frac{\sigma'}{\varepsilon_0} = E \cos\ \delta \tag{1.14}$$

- imaginary part of modulus – loss modulus or modulus out of phase

$$E'' = \frac{\sigma''}{\varepsilon_0} = E \sin\ \delta \tag{1.15}$$

where $E^* = E' + iE''$ is the complex Young elastic modulus (E' and E'' are referred to as storage and loss modulus), $\sigma^* = \sigma' + \sigma''$ and ε^* are complex stress and strain, respectively, ε_0 is a constant. Loss tangens (loss factor) is defined by virtue of the phase shift angle between stress and strain, δ, and related to E' and E'' by

$$\tan\delta = \frac{E''}{E'} \tag{1.16}$$

Storage modulus, E', represents an ideally elastic part of viscoelastic behaviour of the material. It is a measure of the energy stored and recovered per cycle of periodic deformation. The loss modulus, E'', is an extent of mechanical loss in material. It is proportional to the energy dissipated in the form of heat during one cycle. The loss tangent determines such macroscopic properties as the attenuation of propagated waves, the softening of free vibrations and the frequency width of a resonance response. After [23], in the transition zone in all the amorphous polymers, independently on whether they are crosslinked or not, $\tan\delta$ reaches values of loss tangent between 0.2 and 3.

Temperature dependences of all these parameters are often measured. Each material has its own characteristic spectrum of relaxation times during which important processes are completed. To perform quasistatic measurements, sufficiently small temperature rates are necessary. On the other hand, measurements have to be performed in a realistic time. Temperature rates typically 1 – 2 °C/min represent a reasonable compromise and are often in DMA experiments.

Affine versus phantom network model

Equilibrium Young modulus is related to the structure of polymer network. At present, there are many models of polymer network elasticity, however, the oldest ones, namely, phantom [24] and affine [25] model are the most used. They are also referred to as classical models of rubber elasticity.

Both models are based on the following assumptions:

- chain segments between junctions can be represented by Gaussian statistics of phantom chains
- entropy of network is the sum of the entropies of the individual chains
- all conformational states have the same energy
- network in undeformed state is isotropic
- volume of the networks does not change during deformation

However, they differ in the way in which deformation is treated on microscale. In polymer network, all chains are either participating in elastic response (elastically active chains) or are inactive (dangling chains). Elastically active chain is defined as the chain between two network junctions with at least three bonds with infinite continuation (elastically active junctions, see Fig.A.1 in Appendix.) In affine model it is assumed that positions of the junctions in deformed network are changed affinely

in accordance with deformation on macroscale. On the other hand, in the phantom model, this assumption is released and this requirement holds for the junctions located on surfaces of the material. In other words, in the affine model network junctions are not allowed to fluctuate meanwhile in the phantom model they are. Consequently, the phantom network is more compliant than the affine one.

Elastic Gibbs free energy of both, affine and phantom network deformed in x, y, z directions by stretching ratios, $\lambda_x, \lambda_y, \lambda_z$, [22] can be expressed by the same formula

$$G_{el} = \frac{1}{2}kT\left[A\left(\lambda_x^2 + \lambda_y^2 + \lambda_z^2 - 3\right) + B\ln\lambda_x\lambda_y\lambda_z\right] \tag{1.17}$$

where k is Boltzmann constant and T is the absolute temperature and A, B are constants given by

$$A = \nu_{\mathrm{a}} \quad B = \mu_a \qquad \text{affine network}$$

$$A = \xi \qquad B = 0 \quad \text{phantom network}$$

Quantities ν_{a}, μ_{a} and ξ, ($\xi = \nu_{\mathrm{a}} - \mu_{\mathrm{a}}$) are the network parameters (number of elastically active chains, elastically active junctions and cycle rank) and can be calculated using theory of branching process (see Appendix).

Equation 1.17 enables derivation of the relationship between stress, σ, and strain, ϵ, for quasistatic uniaxial extension of polymer networks:

$$\sigma = \frac{A}{V}kT\left(\lambda^2 - \frac{1}{\lambda}\right) \tag{1.18}$$

where V is the volume of the network. For small deformation $\lambda = 1 + \epsilon, \;\; \epsilon \to 0$ and the last equation is reduced to

$$\sigma = 3\frac{A}{V}kT\epsilon \tag{1.19}$$

Comparison of eq.1.19 and 1.13 gives an expression for the Young modulus of affine and phantom network by virtue of the network parameters:

$$E_{\mathrm{aff}} = 3\frac{\nu_{\mathrm{a}}}{V}kT \quad \text{for affine network} \tag{1.20}$$

$$E_{\mathrm{ph}} = 3\frac{\xi}{V}kT \quad \text{for phantom network} \tag{1.21}$$

1.5.5 DSC

The DSC is also one of the techniques of thermal analysis. A heat flow to sample and reference is measured by the device. There are a few variations of DSC instruments (heat flux, power compensated, etc.). In this work the power compensated DSC was used which is the most precise and it is sketched in Fig. 1.8. In the device, there are two microholders, one for the sample, another for the reference, equipped with their own microheaters and platinum thermometers. The principle of the power

compensated DSC consists in keeping zero temperature difference between the sample and the reference. Therefore, when both microholders are heated at a certain heating rate and in one microholder there is a sample, larger amount of heat has to be supplied to its microheater to keep the zero temperature difference. Therefore, heat required to increase the temperature of the sample is directly measured.

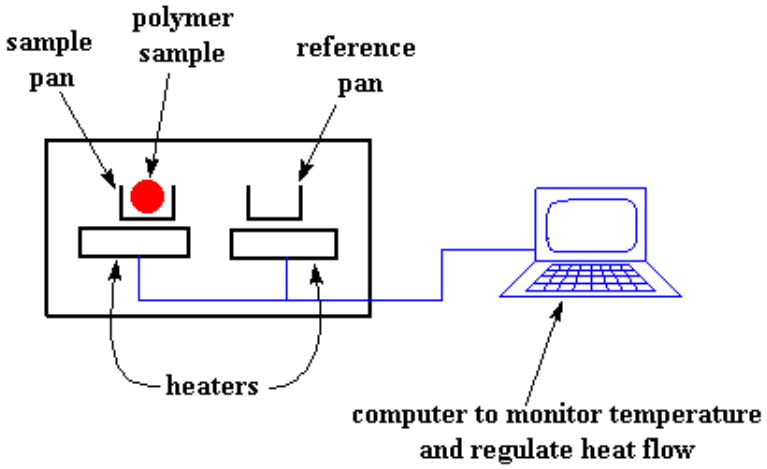

Figure 1.8: Layout of basic differential scanning calorimetry. Reproduced from Ref. [26]

The DSC results are usually represented as heat flow, dq/dt, in dependence on temperature T (thermograms). Small masses of samples are used in the measurement, typically 1 - 50 mg.

In the case of constant temperature rate, the heat capacity is directly proportional to heat flow. The slope of this curve can suddenly change during the experiment indicating some transition in the material. The most important transitions in polymer materials are:

Glass transition region - it is typical for a step in a heat flow curve caused by jump capacity change at T_g. Above the glass transition temperature the sample needs more heat for increasing its temperature at the same rate because releasement of new molecular motions in the material. Thermodynamically, this feature can be explained by equations:

$$C_p(T) = \frac{d\dot{q}}{d\dot{T}}(T) = \frac{\dot{q}}{\dot{T}}(T) \tag{1.22}$$

$$\Delta C_p = \frac{1}{\dot{T}}(\dot{q}_f - \dot{q}_i) \tag{1.23}$$

Fig. 1.9 shows typical DSC thermogram with glass transition step. For the determination of T_g, the two tangents in the beginning and end of transition are marked (black dashed lines). Temperatures, where these lines leave experimental curve, are

designed as T_1 and T_2. They are associated with the width of the transition. The glass transition temperature T_g is often taken as temperature of inflection point between the temperatures T_1 and T_2. The red dashed line crosses experimental curve of heat flow at T_g and follows the curve on both side. Its cross sections with black tangents determine another pair of temperatures T_a and T_b which speak about transition steepness. Correctly, full information about the transition is contained in these five values. However, more frequently, only T_g and Δc_p are reported.

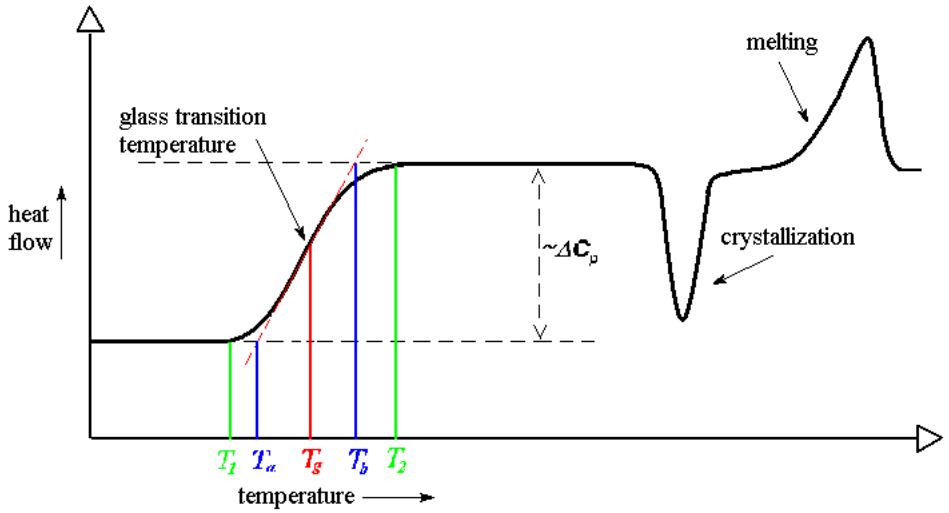

Figure 1.9: Three types of important features of DSC experiments.

Crystallization – above the glass transition temperature, polymer chains gain higher mobility. When the temperature approaches the crystallization temperature of the material, T_c, the chain segments start to form very ordered arrangements, called crystallites. Simultaneously, a heat is released because of immobilization of the chain segments in crystallites which can be seen in the curve as exotherm peak. The crystallization temperature should be determined from the onset of the transition if this is possible. If this is not the case, it is often determined from the position of melting peak. The area under the crystallization peak is equal to latent heat of crystallization (crystallization enthalpy).

Melting – if heating go on further, thermal movement of polymer chains starts to break crystallites formed in the previous stage. Around the melting temperature, T_m, polymer crystals begin to fall apart, the chains come out of their ordered positions and move more freely. An endotherm peak appears in thermogram since energy is consumed in the transition. Both transitions, crystallization and melting, are the first order transition, they have non-zero latent heat. All three processes can be observed on a heat flow versus temperature plot, as we can see in Fig. 1.9.

Before the DSC measurement calibration of the instrument is necessary. The baseline signal to be subtracted from the sample signal is obtained by measurement with empty microholders.

Chapter 2

Objectives

The aim of this work is preparation of polymer hydrogels from epoxy networks and investigation of their structure and properties by a combination of methods. To this purpose a series of hydrophilic epoxy networks is prepared by reaction of α,ω- diamino terminated poly(oxypropylene)-*b*-poly(oxyethylene)-*b*-poly(oxypropylene) with Bisphenol A propoxylate diglycidyl ether (PDGEBA). Network parameters (mass fraction of sol, concentrations of elastically active cahins and junctions, etc.) will be calculated using theory of branching processes. To get information about input parameters for the calculation, network formation process and structure will be monitored by gel permeation chromatography and infrared spectroscopy. Calculated network parameters will be compared with values determined experimentally by extraction and dynamic mechanical analysis. Presence (absence) of phase separation in the networks will be verified by dynamic mechanical analysis and differential scanning calorimetry. Epoxy hydrogels will be prepared by swelling of the networks in water and their structure on nanometer length scale will be investigated using small-angle neutron scattering. Elastic and thermal behaviour of hydrogels will be also studied by dynamic mechanical analysis and differential scanning calorimetry.

Chapter 3

Experimental

3.1 Materials

In the preparation of networks α,ω-diamino terminated poly(oxypropylene)-*b*-poly (oxyethylene)-*b*-poly(oxypropylene) (Jeffamine ED600, Huntsman) and Bisphenol A propoxylate diglycidyl ether(PDGEBA, Sigma-Aldrich)were used. Chemical structure of both reactives is shown in Figs. 3.1 and 3.2. Molar mass of ED600 is ca 600 g.mol^{-1} and POE content is ca 60 wt.%. Molar concentrations of amino groups in ED600 and epoxy groups in PDGEBA determined by titrations were $c_{\mathrm{NH2}} = 3.2 \times 10^{-3}$ mol.g^{-1} and $c_{\mathrm{E}} = 2.92 \times 10^{-3}$ mol.g^{-1}, respectively [31]. Series of epoxy networks was prepared, at compositions described by stoichiometric ratio, r, defined as initial molar ratio of reactive groups:

$$r = 2\frac{[\mathrm{NH_2}]_0}{[\mathrm{E}]_0} \tag{3.1}$$

Values of r in the series changed from $r = 1$ (stoichiometric network) to 2 (see Table 3.1).

Sample	r	w_{S}	w_{POE}	w_{POP}	w_{PDGEBA}
EP 111	1.00	0.05	0.188	0.125	0.687
EP 112	1.06	0.04	0.195	0.130	0.675
EP 113	1.12	0.04	0.203	0.135	0.662
EP 114	1.25	0.06	0.218	0.145	0.637
EP 115	1.50	0.12	0.244	0.162	0.594
EP 116	1.75	0.17	0.266	0.177	0.556
EP 117	2.00	0.25	0.286	0.191	0.523

Table 3.1: Parameters of epoxy networks prepared, r is the stoichiometric ratio, w_{S} is the mass fraction of extractable sol, w_{POE}, w_{POP} and w_{PDGEBA} are the mass fractions of poly(oxyethylene), poly(oxypropylene) and diepoxide.

At the begiining, the both reactives were stirred at 100 °C for about 15 min and then poured into polypropylene moulds. Curing reaction of all systems proceeded

at 120 °C for 48 h in nitrogen atmosphere. Samples of the networks in the form of sheets of thickness ca 1 mm were obtained. All the sheets were transparent.

After the preparation, the networks contain a certain amount of extractable part (sol) which has to be removed before swelling and SANS measurements. This was realized by extraction of the samples in good solvent (toluene) at room temperature (24 hrs, three times). Values of mass fraction of sol, w_S, was determined from masses of the samples before and after extraction and are also given in Table 3.1.

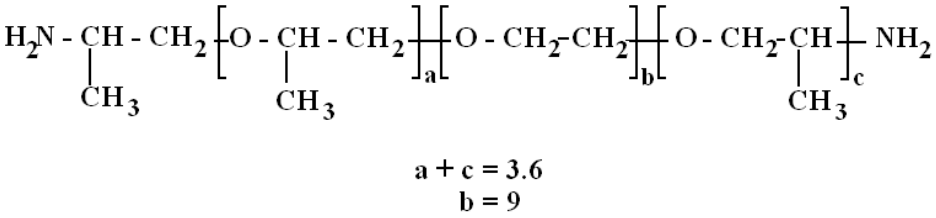

Figure 3.1: Chemical structure of Jeffamine ED600.

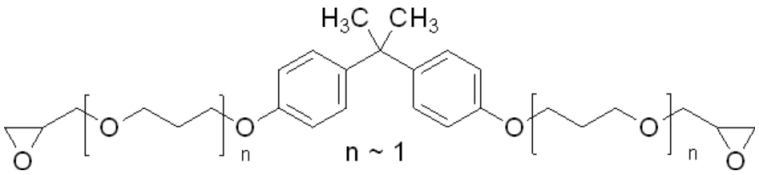

Figure 3.2: Chemical structure of PDGEBA. Reproduced from Ref. [27].

Gels and hydrogels were prepared by swelling of circular specimens cut from dry extracted networks in solvent (methanol and water). The size of samples depended on the method of investigation, diameters typically of ca 20 - 30 mm were used for SANS and swelling degree determination. After immersion of the network samples in solvent they were allowed to achieve equilibrium which took ca 2 days.

3.2 Measurements

GPC measurements were performed using chromatograph LABIO equipped with 600 x 7.5 mm PL gel column of porosity 500 (Polymer Laboratories), and differential refractive index detector. Tetrahydrofuran was used as mobile phase (eluent) at flow rate 1 mL/min. Before the measurement, the column was calibrated using polystyrene standards of narrow polydispersity. Samples to be measured were dissolved in a necessary amount of 2 % solution of toluene in THF[1] to obtain ca 5 % (w/v) solutions.

Infrared absorption spectra were collected using a Thermo Scientific Nicolet 6700 FTIR spectrometer in the range of 4000-500 cm^{-1} by ATR method with ZnSe crystal. A resolution of 1 cm^{-1} was used in the acquisition of all spectra, and 64 scans

[1]Toluene is used as internal standard for GPC measurement.

were signal-averaged to achieve a good signal-to-noise ratio. There was no need to additional spectrum corrections such as ATR correction for elimination of influence of higher scattering at lower frequency or subtracting of background.

The SANS experiments were realized on the small-angle neutron scattering diffractometer called 'Yellow Submarine' operating on cold neutron beam line at the Budapest Research Reactor [28]. Two sample - detector distances (1.3 m and 4 m) and mean neutron wavelength $\lambda_n = 4.1$ Å were used, so as the range of the magnitudes of scattering vector $q = 0.01$ - 0.36 Å was covered. Temperature during scanning was hold at 25.0±0.1 °C. The primary neutron beam is moderately polychromatic (due to the transmission function of the velocity selector), with normal distribution of wavelength and standard deviation, $\Delta\lambda_n/\lambda_n \approx 0.08$–$0.11$, [28]. In the evaluation of SANS data, the polychromaticity was taken into account. Two series of samples were investigated using SANS instrument: epoxy networks swollen in deuterated solvents (D_2O and CD_3OD). The samples swollen to equilibrium were closed between two quarts windows separated by a sealing from silicone rubber and mounted into aluminium holders before the measurements. The scattering intensities were radially averaged and corrected for the sample transmission, room background and detector efficiency using standard procedures.

Dynamic mechanical analysis was performed using a Seiko DMS210 Analyzer. Rectangular strips having dimensions ca 25 mm × 9 mm × 1 mm were cut from the sheets of networks prepared. The strips were suspended between two clamps and measured in uniaxial extension at heating rate 2 °C/min from -70 to 70 °C. To obtain temperature dependences of storage and loss moduli samples were measured at a constant frequency of (0.1 Hz, 1 Hz). Before the measurements samples were dried at 40 °C in vacuum for 24 hours and then kept in a dessicator to prevent air-moisture contamination.

Stress-strain characteristics of hydrogels were measured using a Perkin-Elmer DMA7e analyser at 25 °Cr. Rectangular strips of dimensions ca 15 mm × 4 mm × 1 mm) were cut from the hydrogel samples and measured immersed in water in uniaxial extension at constant force rate (40 mN/min).

Thermograms of samples were obtained using a Perkin-Elmer Pyris 1 differential scanning calorimeter. The instrument was calibrated according to standard procedures using mercury and indium as standards. Nitrogen at flow 20 mL/min was used as a purge gas. Samples of ca 10 - 53 mg were sealed in aluminium pans and measured in cooling at 10 °C/min from 30 °C (hydrogels) or 50 °C (networks) to -55 °C, followed by temperation at - 55 °C for 5 min and heating at 10 °C/min to 50°C (hydrogels) or 100 °C (networks).

Specific mass of the samples was determined by the method of double weighing (on air and in ethanol) using pieces of prismatic shape of dimensions ca 8 mm × 9 mm × 1 mm. The value of the specific mass was determined as an average over three samples.

Chapter 4

Results and discussion

4.1 Characterization of the reactives used

First, both reactives, PDGEBA and ED600, were investigated by GPC. Mass distribution of molar mass obtained for PDGEBA is given in Fig. 4.1.

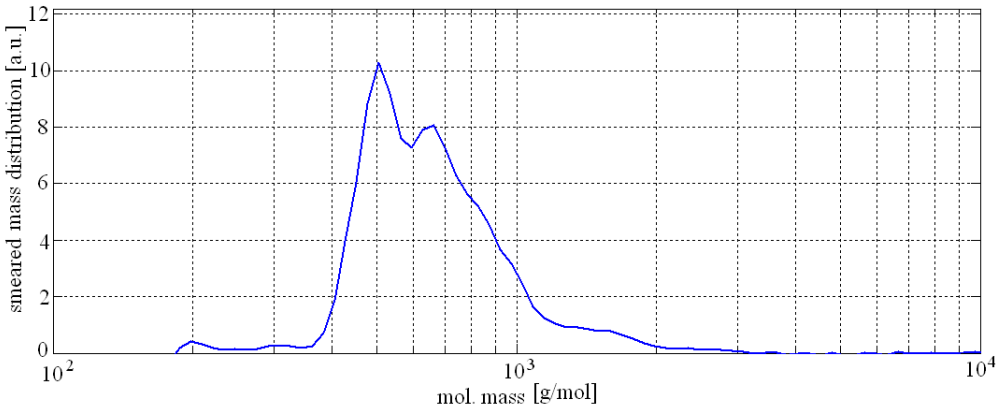

Figure 4.1: Mass distribution of molar mass obtained for PDGEBA by GPC.

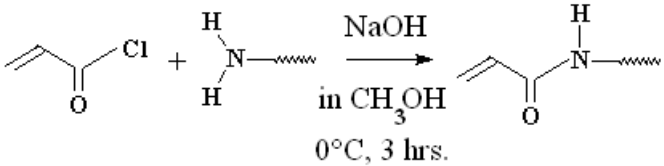

Figure 4.2: Modification of ED600 in reaction with acryloyl chloride.

Two peaks centered at ca 500 and 650 g/mol, respectively, can be seen. The difference in molar mass is about 150 g/mol which would correspond to ca two oxypropylene units (M_{OP} = 58 g/mol), however, this number may be lower since the chromatograph was calibrated using polystyrene. The only conclusion from this experiment is: PDGEBA consists of two fractions differing probably in number of

oxypropylene units located between benzene rings and epoxy rings (see chemical formula of PDGEBA in Fig. 3.2).

Surprisingly, GPC measurement of ED600 did not show any signal from the solute. A too small difference in refractive indices of the ED600 solution and elution solution (2 % (v/v) of toluene in THF) is a probable reason for failure of this method. To obtain GPC signal, amino groups on ED600 were converted by reaction with acryloyl chloride to acrylamido groups (see Fig. 4.2). Mass distribution obtained for α, ω- diaminoacryloyl terminated ED600 is given in Fig.4.3

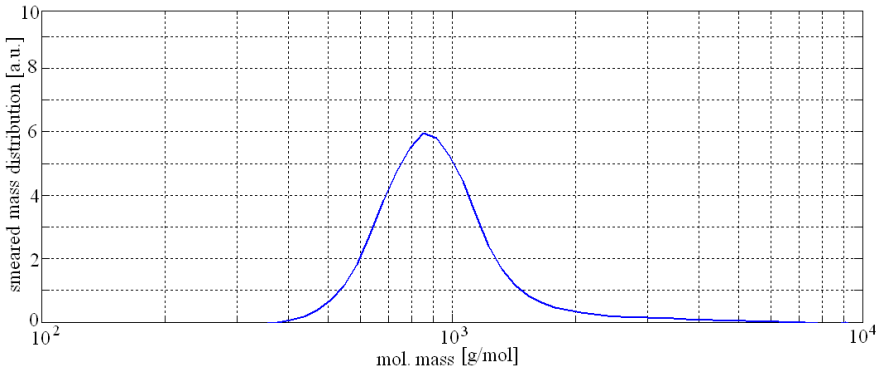

Figure 4.3: Mass distribution of molar mass obtained for α, ω- diacrylamido terminated ED600 by GPC.

A single peak in centred around ca 850 g/mol was obtained. This value is close to the molar mass expected for α, ω- diaminoacryloyl terminated ED600 (ca 700 g/mol).

Chemical structure of the reactives was also investigated by FTIR. Fig. 4.4 and 4.5 show the spectra of PDGEBA and ED600, respectively. The spectra are complex, especially in fingerprint region. Bands providing some information about network formation process will be addressed, only, a more detailed interpretation of spectra is out of scope of this work.

In the spectrum of PDGEBA (see Fig. 4.4), at 3044 cm^{-1} a band from the C-H stretching from benzene rings can be seen followed by a multiple peak in the region from 2880 to 3050 cm^{-1} attributed to the C-H stretching. Among many bands in the lower wavenumbers region, an important peak at 1248 cm^{-1} from the epoxy ring breathing (symmetric all ring stretching) can be seen. In the region from 1030 to 1820 cm^{-1}, there are also many peaks attributed to the aliphatic C-O-C bending.

As regards ED600, few bands attributed to the antisymmetric (3370 cm^{-1}) and symmetric (3300 cm^{-1}) N-H stretching from terminal amino groups are located at highest wavenumbers, followed by an intensive peak from stretching of C-H in (abundant) methyl and methylene groups of POE and POP blocks. Among many bands in the lower wavenumbers region, we will mention just a band from the N-H bending located at 1584 cm^{-1} and an intensive peak centered at 1093 cm^{-1} from the antisymetric vibrations of C-O-C from ED600 backbone.

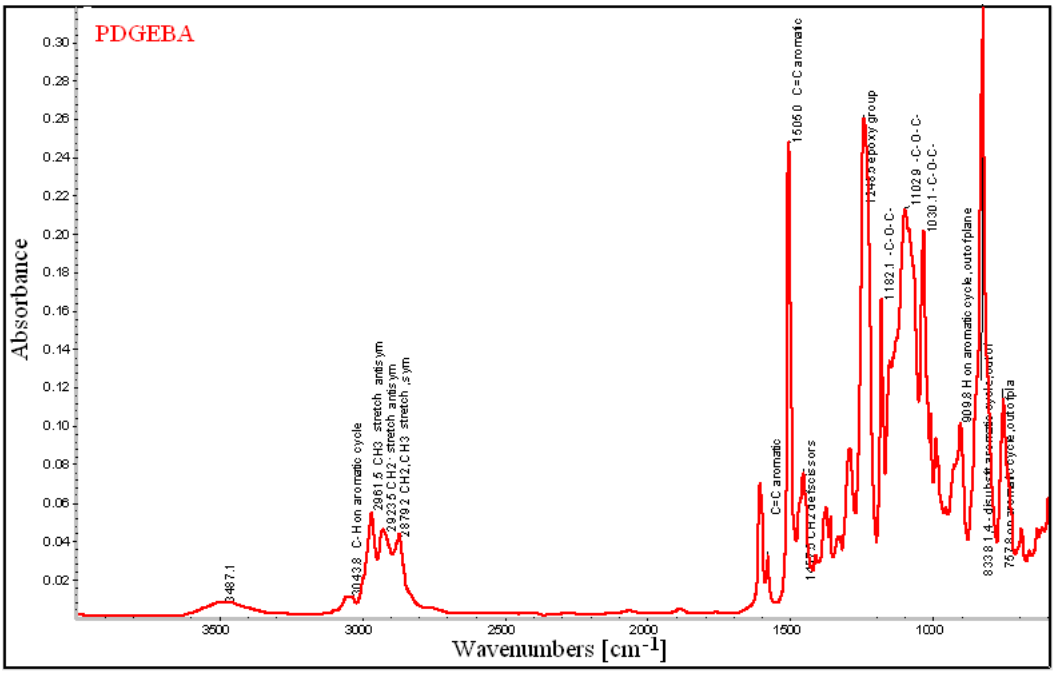

Figure 4.4: ATR-FTIR spectrum of PDGEBA measured at 25 °C.

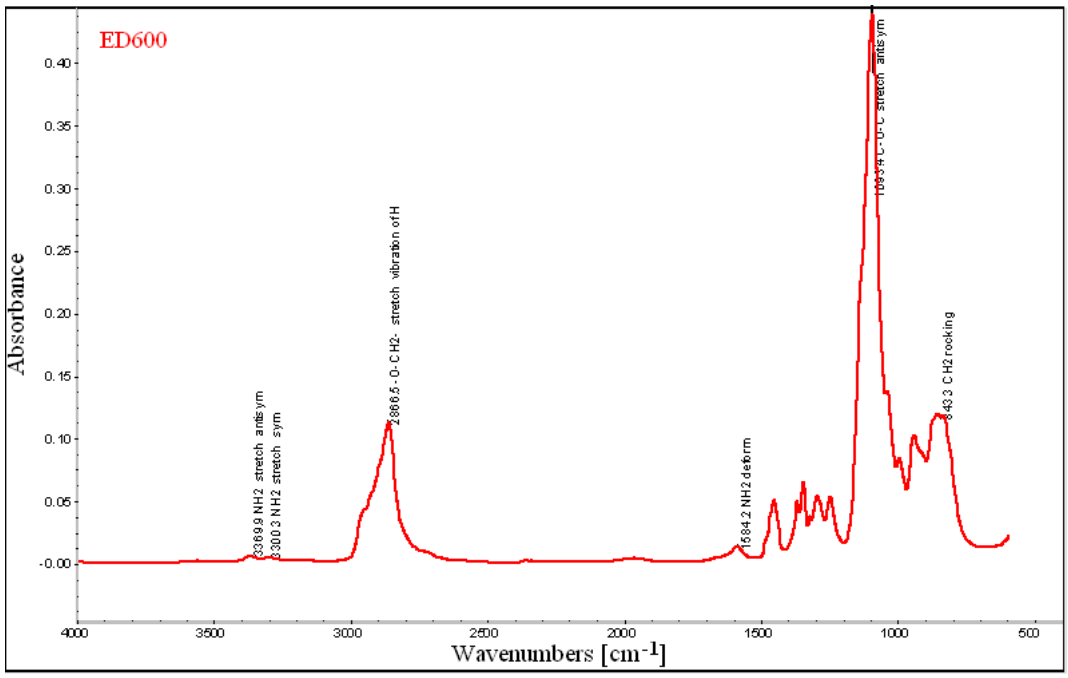

Figure 4.5: ATR-FTIR spectrum of ED600 measured at 25 °C.

4.2 Study of the epoxy network formation

Network formation process determines final architecture of the polymer network. To this purpose a combination of GPC and FTIR was employed. Due to impossibility to obtain a GPC signal from ED600 solutions in THF, a similar system has to be chosen in investigated of the network formation process, namely, mixture of another diamine (Jeffamine D2000) and PDGEBA[1]. Jeffamine D2000 is α,ω- diamino terminated poly(oxypropylene) of number average of molar mass ca 2000 g/mol.

For the measurements, ca 2 mL of stoichiometric mixture of D2000 and PDGEBA was prepared in a 4 mL vial at room temperature and then transferred into an oil bath thermostated at 120 °C. Small amounts from the mixture were withdrawn successively and used in GPC and FTIR measurements. For GPC, 5 % (w/v) solutions of the reaction mixture in 2 % (v/v) mixture of toluene in THF were prepared. They were being withdrawn until the gel point was achieved (at ca 160 min of the reaction). In the gel point the reaction mixture became solid and small pieces from it were cut to be used in FTIR, only.

Time evolution of mass distribution of molar mass in the reaction mixture determined from chromatograms is shown in Fig. 4.8. At the beginning of the reaction, the distribution is just a superposition of the contributions from D2000 and PDGEBA. Both peaks from PDGEBA decrease in intensity with reaction time which means that both fractions in PDGEBA are consumed in the reaction. The peak from D2000 is overlapped quickly by a peak from an oligomer of molar mass ca 2600 g/mol. A progressive formation of heavier oligomers at the expense of smaller ones can be seen very well. Detection of species of the molar mass higher than ca 50 000 g/mol is behind resolution capacity of the GPC column used.

Conversion of epoxy groups at the gel point is ca 60 % as estimated by comparing area below peaks attributed to PDGEBA. This value is somewhat higher than the value predicted for equal reactivity of amine hydrogens (ca 58 %, see Fig. 4.6) approving a lower reactivity of hydrogens from secondary amines (a strong substitution effect) in the system studied. This finding is supported by the oligomer population found by GPC consisting mainly of linear species (see Fig. 4.8).

In the case of strong substitution effect linear oligomers are formed preferentially in the beginning of the reaction. An example of such structures expected in the system studied are sketched in Fig. 4.7. Location of GPC signals from the linear oligomers is denoted in Fig. 4.8 by short vertical lines. The signals for oligomers of molar mass higher than 5.10^4 g/mol are not shown because the GPC column used is not able to resolve them.

[1] A diamine of molar mass closer to ED600 produced by Huntsman - D400 - could not be used since it is not miscible with PDGEBA at the temperature of curing (120 °C).

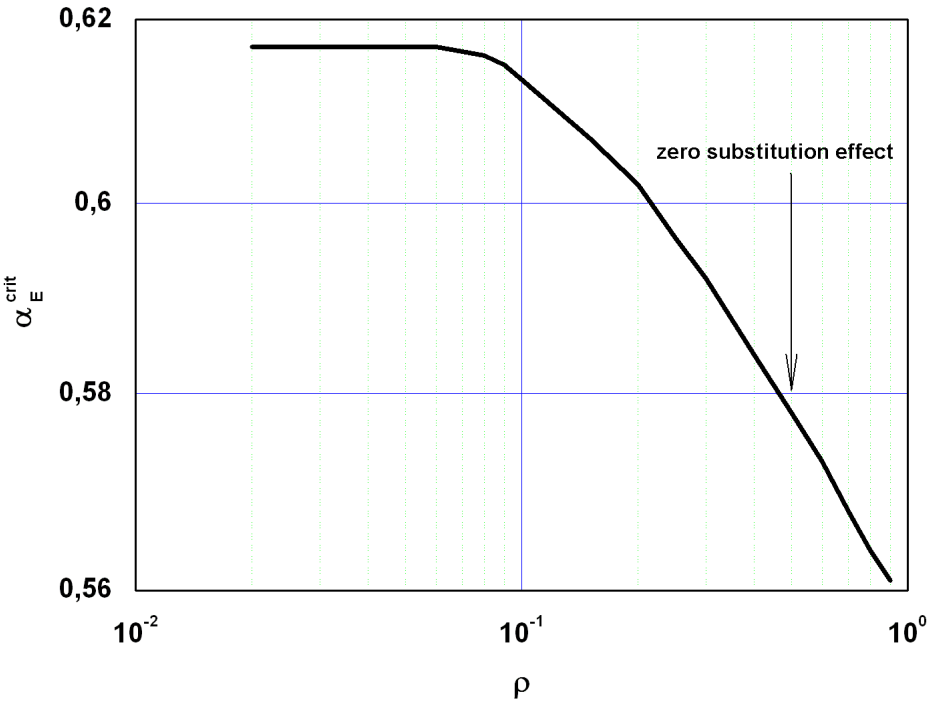

Figure 4.6: Theoretical dependence of the critical conversion of epoxy groups in the stoichiometric mixture of a diamine and a diepoxide as a function of the relative reactivity of secondary to primary amino groups. Reproduced from Ref. [11].

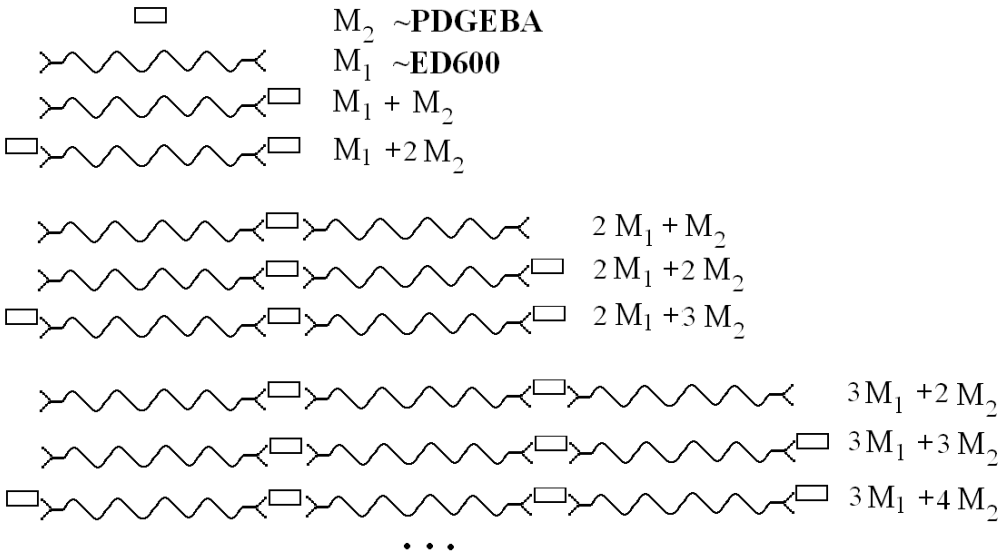

Figure 4.7: Schematic of oligomers and their masses that would appear in the beginning of polymerization considering the strong substitution effect.

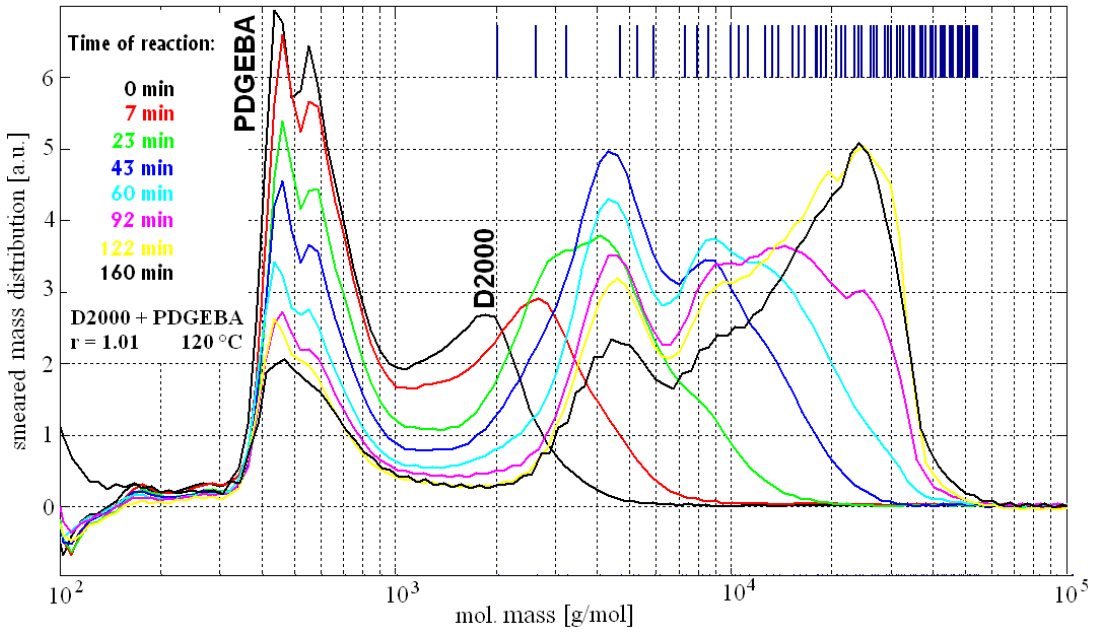

Figure 4.8: Time evolution of mass distribution of molar mass in the stoichiometric mixture of D2000 and PDGEBA reacting at 120 °C. Short vertical lines denote expected positions of GPC signals from linear oligomers containing up to 20 diamine molecules that would appear during polymerization in the case of strong substitution effect (see Fig. 4.7).

Network formation was also investigated by FTIR. Fig. 4.9 shows FTIR spectrum of D2000. Infrared bands assignment for D2000 is similar to that for ED600, one important difference is that bands from vibrations of N-H are much smaller due to higher molar mass of D2000. Bands from the C-H stretching in methyl groups are much more intensive in D2000 relative to ED600 because it consists of oxypropylene units, only.

Drops withdrawn from the reaction mixture were cooled down at a glass slab first, then transferred on ZnSe crystal and submitted to the ATR-FTIR measurement. Disappearance of absorption bands originating from amino and epoxy groups vibrations and appearance of bands from hydroxy groups is expected in the spectra with progressing reaction. Positions of these bands are given in Table 4.1.

ν [cm^{-1}]	Group of atoms	Type of vibration
1245	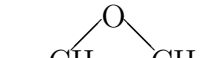	symmetric whole-ring stretching
908		antisymmetric half-ring stretching
3368	$-NH_2$	antisymmetric stretching
3300	$-NH_2$	symmetric stretching
1591	$-NH_2$	bending
3200 – 3600	–OH	stretching from hydrogen-bonded OH multimers

Table 4.1: Infrared assignments for important bands.

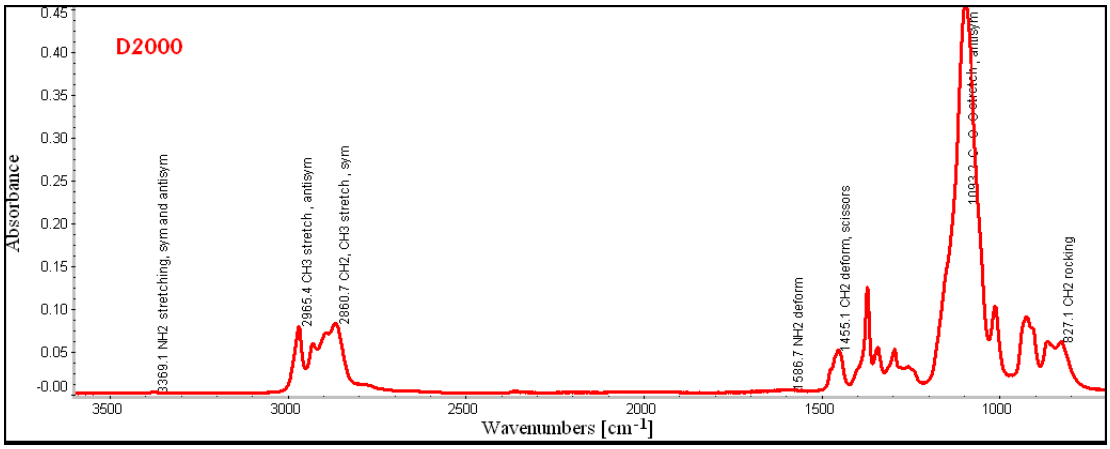

Figure 4.9: ATR-FTIR spectrum of D2000 measured at 25 °C.

In Figure 4.10, a band from the O-H stretching increasing with reaction time can be seen. Hydroxy groups are product of the reaction of epoxy and amino groups (see Fig. 1.2). In Figure 4.11 a decreasing band at ca 908 cm^{-1} from antisymmetric half-ring stretching of epoxy group is also apparent.

Infrared spectroscopy was also used to find an information about completness of the curing reaction in epoxy networks prepared. In the reaction, amino and epoxy

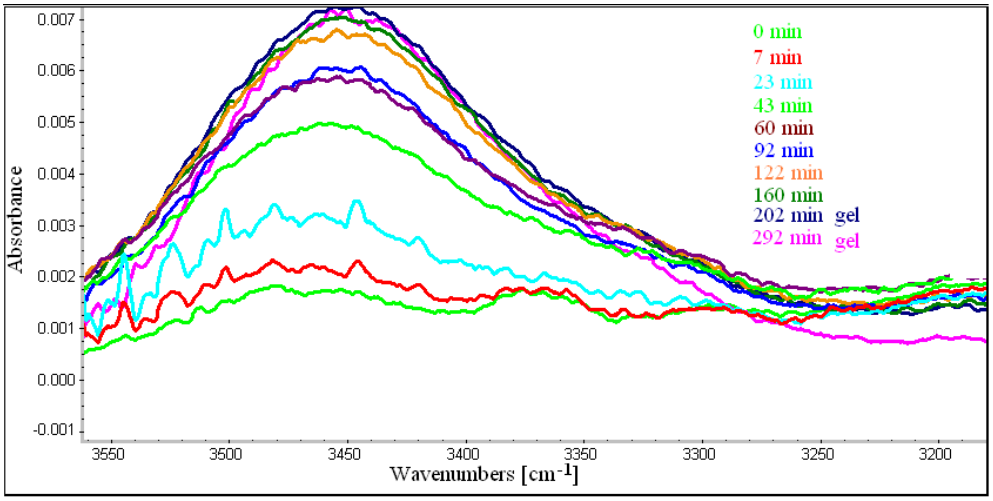

Figure 4.10: Time evolution of ATR-FTIR spectra in the region 3600 - 3150 cm^{-1} of stoichiometric mixture of D2000 and PDGEBA measured during polymerization. The last two spectra are obtained after gellation of the system.

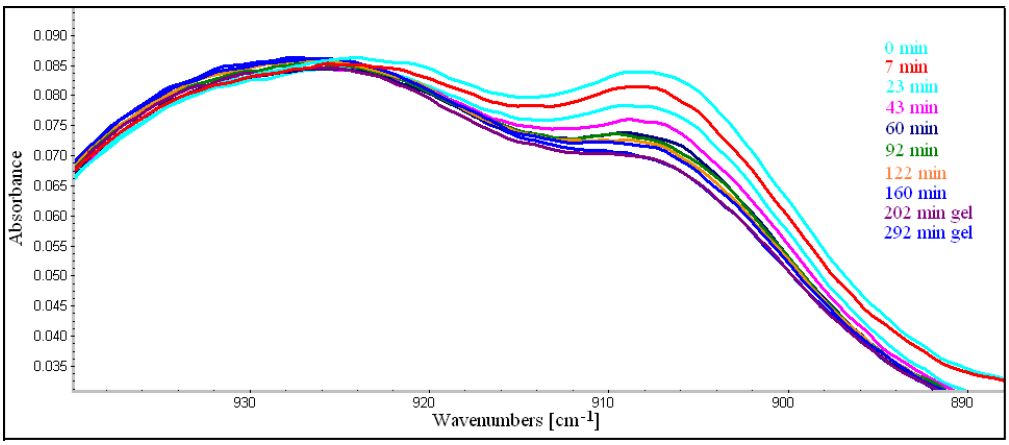

Figure 4.11: Time evolution of ATR-FTIR spectra in the region 940 - 880 cm^{-1} of stoichiometric mixture of D2000 and PDGEBA measured during polymerization. The last two spectra are obtained after gellation of the system.

groups are consumed and hydroxy groups are formed, respectively. All the networks were prepared in excess of amino groups, therefore, if full conversion of epoxy groups were achieved the infrared bands originating from epoxy groups should be missing in the spectra obtained from the networks.

Fig. 4.12 compare the infrared spectra of ED600, PDGEBA and extracted epoxy networks in the 3700-3100 cm^{-1} region. Unfortunately, the results obtained in this region are not helpful to answer the above question since band from the N-H stretching is overlapped with the appearing band from O-H stretching.

In Fig. 4.13 infrared spectra in the region from 1280 to 1160 cm^{-1} are shown. A band at 1250 cm^{-1} is presented in both PDGEBA and ED600 spectra and can be assigned to the aliphatic C-O-C bending. This band should remain in spectra obtained also for the networks and this is confirmed. Bands at 1235 cm^{-1} and 1185 cm^{-1} are due to symmetric whole-ring stretching of epoxy group and present only in spectra of PDGEBA. They should disappear from spectra of the networks in the case of full conversion of epoxy groups. This is not case as is obvious from the Fig. 4.13. Unfortunately, to obtain quantitative information about the conversion of epoxy groups a calibration of the band would be necessary. However, a study of kinetics of epoxy curing was not aimed in this work.

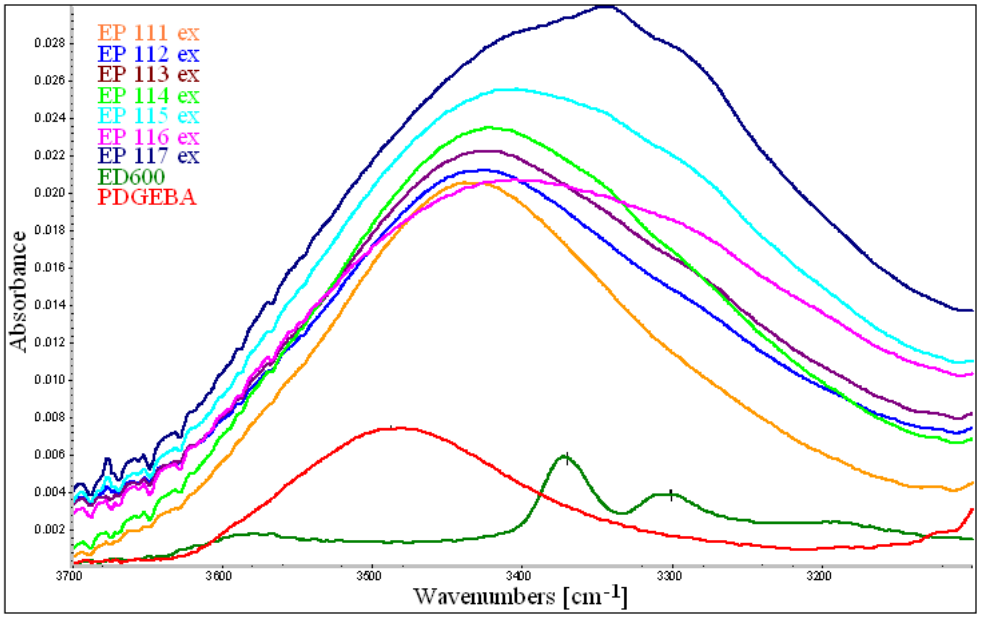

Figure 4.12: ATR-FTIR spectra in the 3700 – 3100 cm^{-1} region of ED600, PDGEBA and extracted networks.

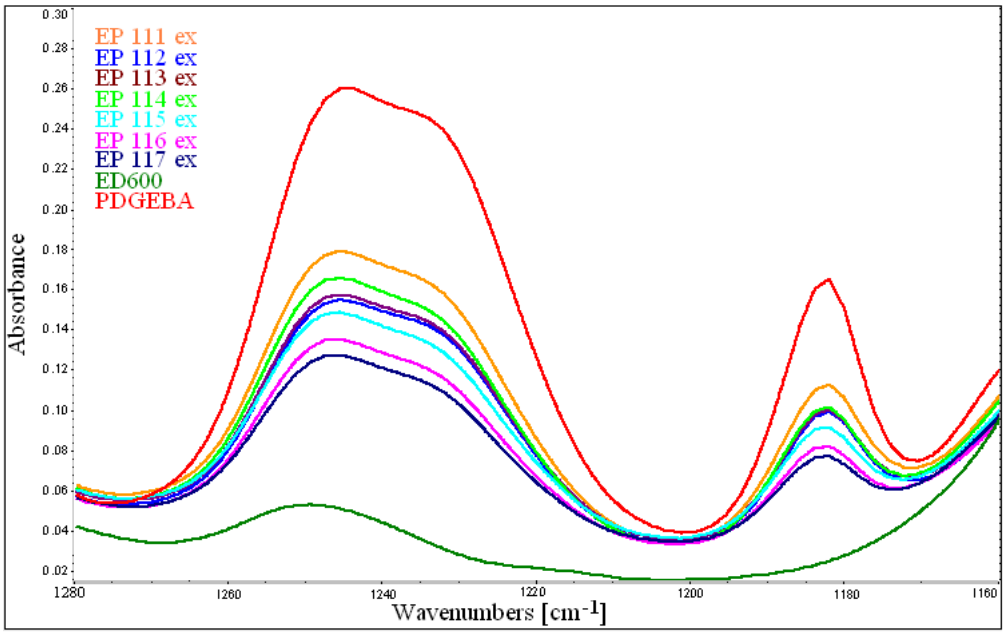

Figure 4.13: ATR-FTIR spectra in the 1280 - 1160 cm^{-1} region of ED600, PDGEBA and extracted networks.

4.3 Epoxy networks

4.3.1 Mechanical properties

Dynamic mechanical properties of the networks were carried out in extension mode at frequency $f = 1$ Hz and $f = 0.1$ Hz (dynamic experiment). Temperature dependences of storage Young modulus, E' and loss tangent, $\tan\delta$ obtained for non-extracted samples and extracted samples are shown in Figures 4.14 and 4.15, respectively.

All samples exhibit a single glass transition at temperature in range from -8 to 7 °C. The curves are similar in shape, but horizontally or vertically shifted and differ in width of the transition. Elastic modulus in rubbery state decreases with increasing stoichiometric ratio, r, for both extracted and non-extracted samples, however, for the networks with r close to 1 the values of elastic modulus are almost equal. In the glassy state, the situation for non-extracted networks is reverse, the networks with higher r show lower values of elastic modulus. The higher r the bigger difference between curves appears at increased temperatures which may be also due to logarithmic sampling. These observations were confirmed by repetition of the experiments, the results were almost identical.

The glass transition temperatures of non-extracted and extracted networks, T_α, determined from loss tangent maximum at frequency $f = 1$ Hz decrease with increasing r in both series (see Figure 4.17). The values of T_α for all the extracted networks, except EP 117ex, are higher than for non-extracted. The probable reason is that fraction of the component with lower glass transition temperature, ED600 (T_g ca -60 °C), in extracted networks is somewhat lower. The width of the transition increases with increasing of r.

Sample	r	E'_{60} [MPa]	d [g.cm^{-3}]	T_α [°C]
EP 111	1.00	2.86	1.153	3.5
EP 112	1.06	2.87	1.152	3.0
EP 113	1.12	2.87	1.152	2.6
EP 114	1.25	2.81	1.152	2.1
EP 115	1.50	1.46	1.151	-1.2
EP 117	2.00	0.59	1.145	-7.1
EP 111 ex	1.00	3.54	1.152	6.3
EP 112 ex	1.06	3.74	1.146	5.2
EP 113 ex	1.12	3.65	1.150	5.1
EP 114 ex	1.25	2.56	1.153	3.0
EP 115 ex	1.50	1.22	1.150	-0.7
EP 117 ex	2.00	0.97	1.151	-7.9

Table 4.2: DMA characteristics of epoxy networks: the storage Young modulus, E', at $T = 60$°C ($f = 1$ Hz), the specific mass, d. The r denotes the stoichiometric ratio.

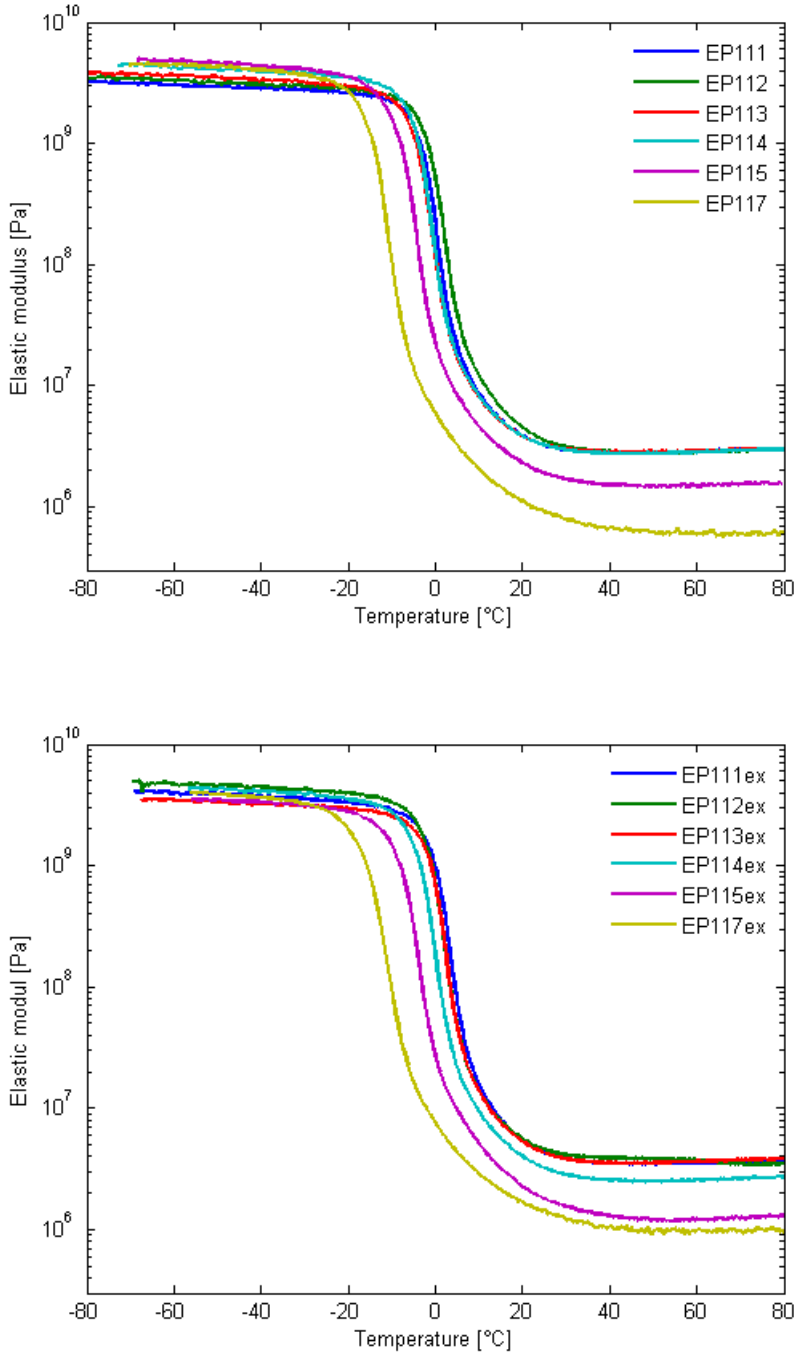

Figure 4.14: Elastic storage modulus, E', of non-extracted (upper) and extracted (down) samples as a function of temperature obtained in dynamic experiment at frequency f= 1 Hz.

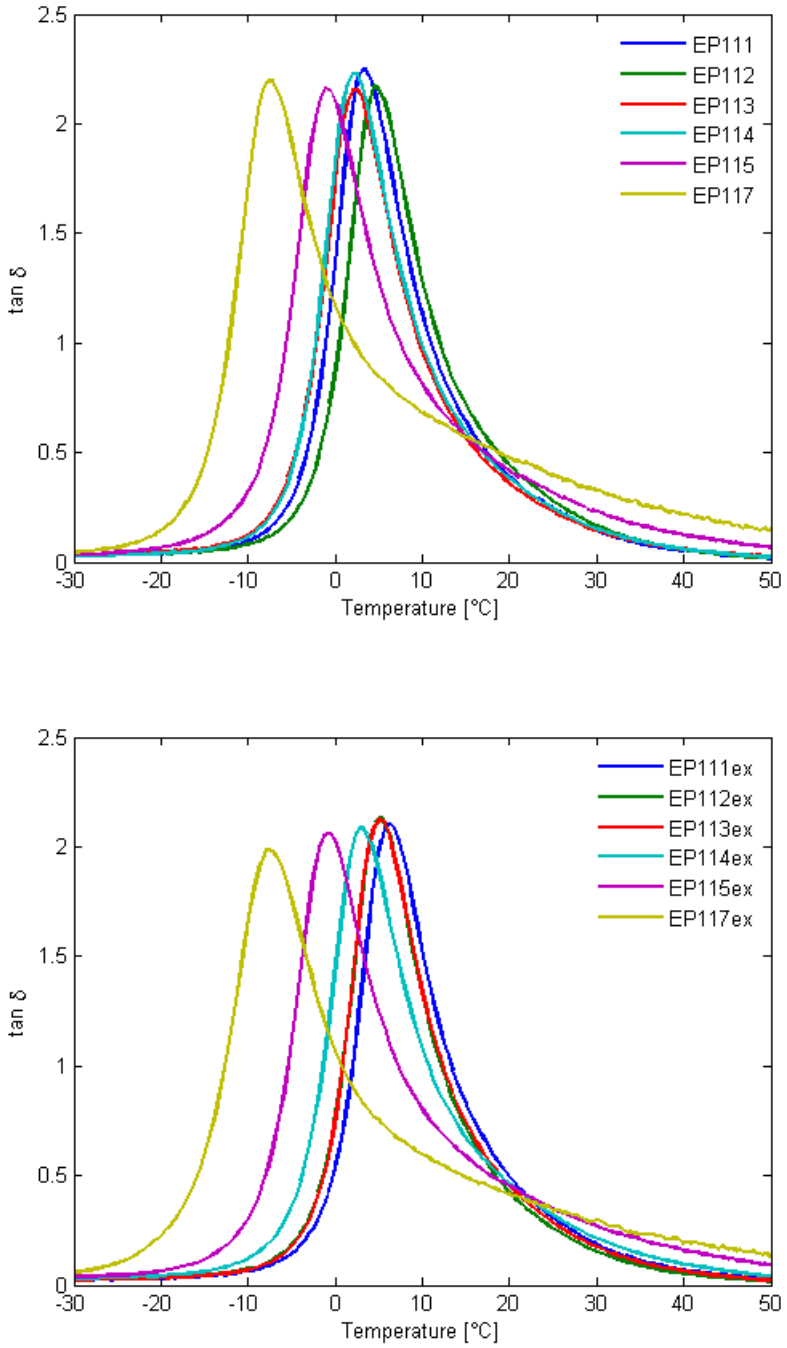

Figure 4.15: Tangent delta of non-extracted (upper) and extracted (down) samples as a function of temperature obtained in dynamic experiment at frequency $f = 1$ Hz.

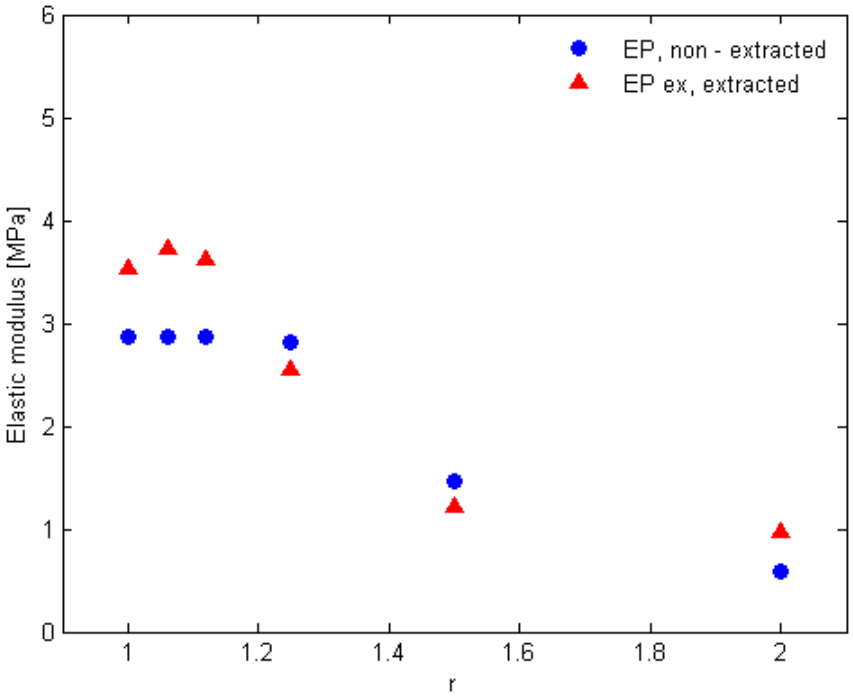

Figure 4.16: The storage Young modulus, E', obtained at $T = 60°C$ and $f = 1$ Hz as a function of stoichiometric ratio, r, for non-extracted and extracted samples detremined by DMA.

Comparison of the values of storage Young modulus determined at 60 °C and f=1 Hz for non-extracted is illustrated in Figure 4.16.

Extracted networks have higher Young modulus in rubbery state than non-extracted ones because concentration of elastically active network chains is increased when sol is removed by extraction and volume of the system is reduced.

Similar trends were found by Fernandez and co-workers [29] who studied mechanical properties of epoxy networks prepared from diglycidyl ether of Bisphenol A (DGEBA) and poly(oxypropylene)diamine with stoichiometric ratio r varying from 0.6 to 1.4. The authors carried the measurement in three-point bending mode at frequency $f = 10$ Hz. The glass transition temperature was highest for stoichiometric network.

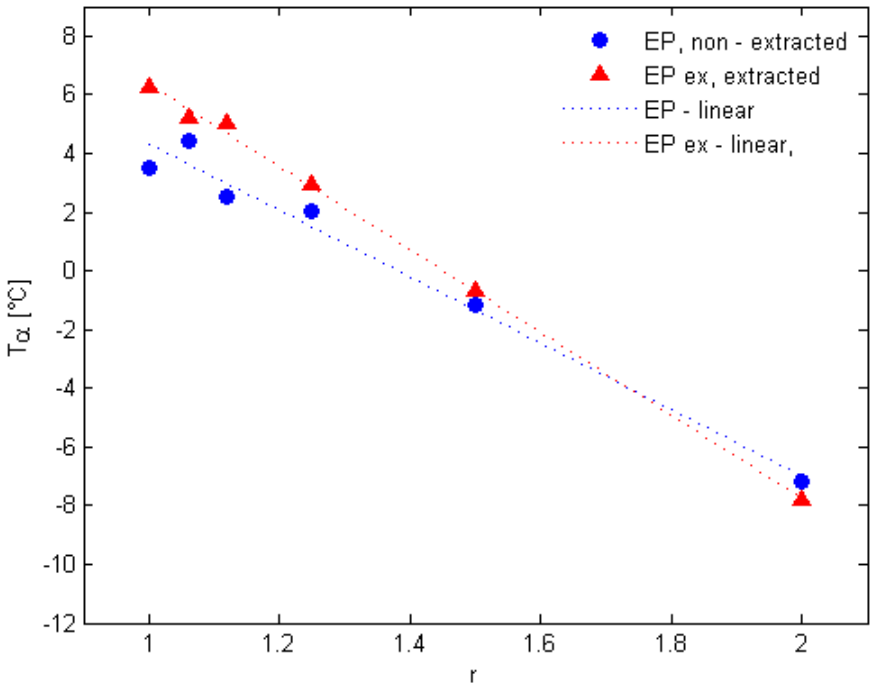

Figure 4.17: The glass transition temperatures, T_α, as a function of stoichiometric ratio, r, for non-extracted and extracted samples determined by DMA at $f = 1$ Hz.

4.3.2 Comparison with the results from theory of branching processes

The theory of branching processes (see appendix A) allows calculation of many network parameters, e.g., mass fraction of sol, w_S, cycle rank, ξ and numbers of elastically active chains, ν_a and junctions, μ_a. Mass fractions of sol can be determined directly, the remaining network parameters are compared using reduced elastic modulus (see eq. A.22).

In Fig. 4.18 a comparison of experimental values and those calculated using theory, eq.A.12 (in Appendix), is given. Effects of conversion of epoxy groups, α_E, at zero substitution effect and the strength of the substitution effect, ρ, respectively, can be seen in Fig. 4.18 (a) and (b). The best agreement is obtained for values $\rho = 0.5$ and $\alpha_E = 0.90$ which seems to be in contradiction with results from stoichiometry. The difference may be due to uncomplete extraction of the networks with higher r.

Fig. 4.19 shows a comparison of reduced experimental, affine and phantom Young modulus (E_{red}, E^{aff}_{red} E^{ph}_{red}). The dependences for affine network are calculated for two cases: diamine is considered either as four-functional junction (rigid) or as a chain between two three-functional junctions (flexible). Phantom network is not influenced by this definition. The best regards are obtained again for uncompleted reaction (α_E=0.90) and phantom model.

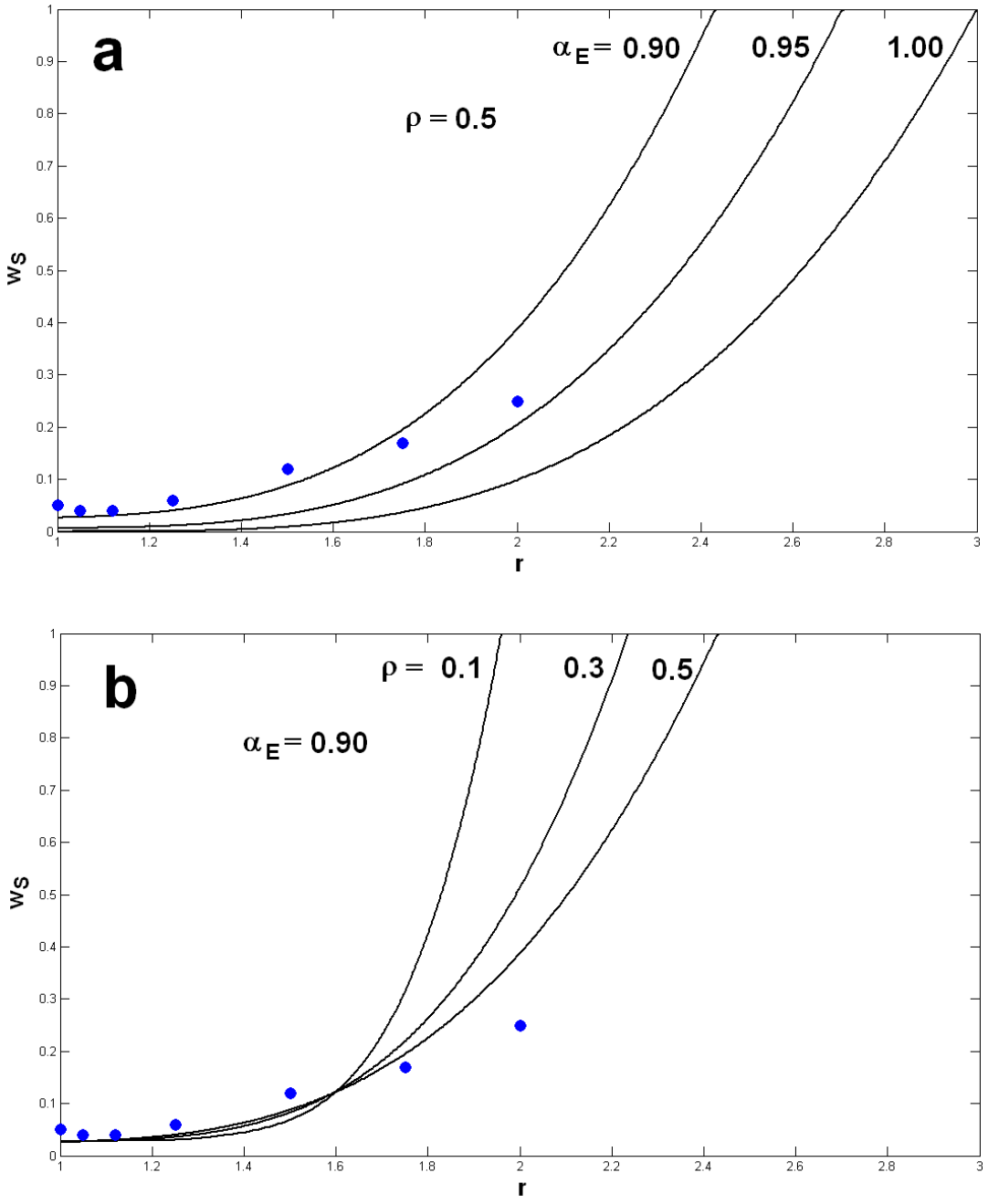

Figure 4.18: Comparison of experimental (full circles) and theoretical values of mass fraction of sol. In the figures eighter the conversion of epoxy groups, α_{E}, or parameter defining the strength of the substitution effect, ρ, varies at constant value of the other constituent.

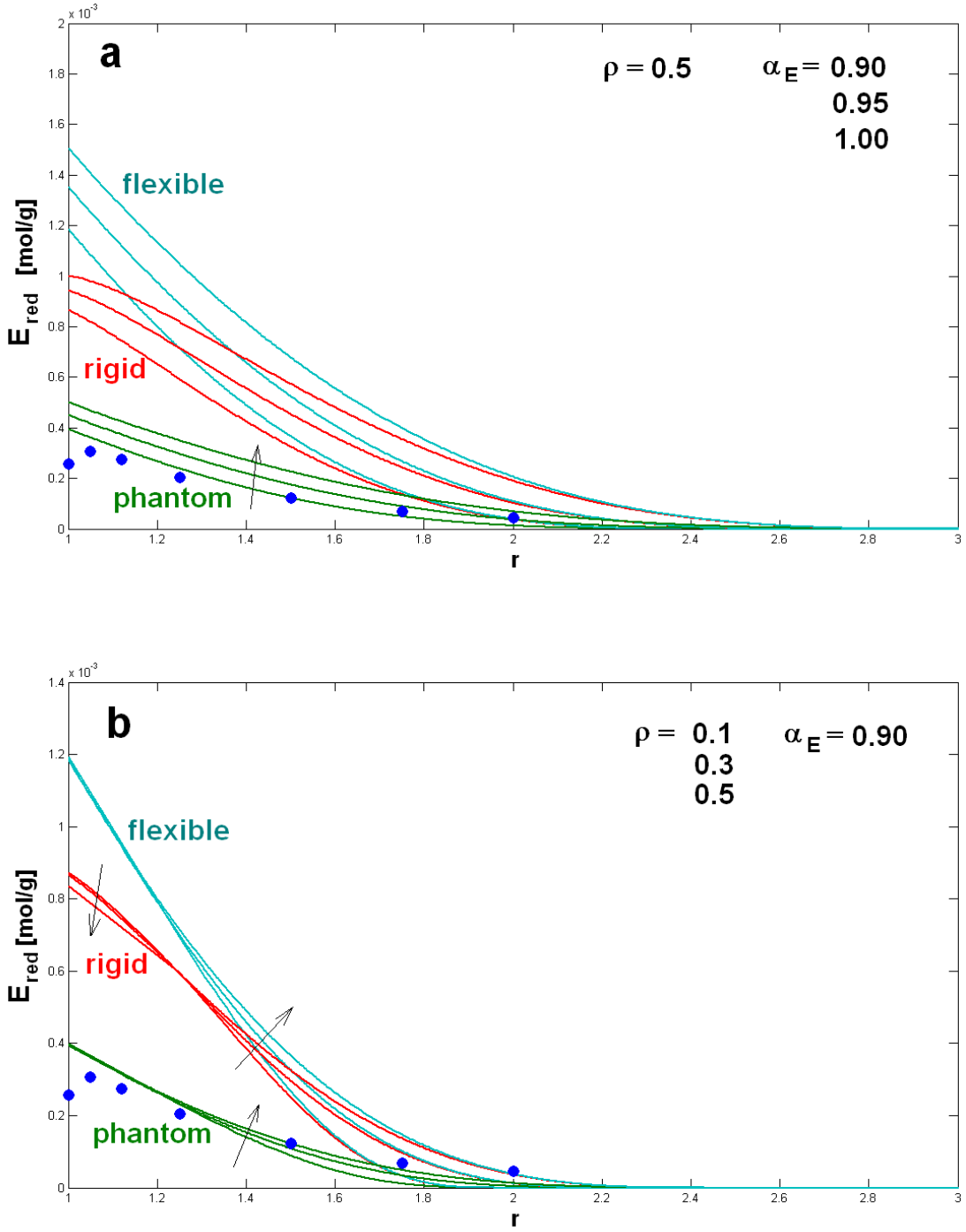

Figure 4.19: Comparison of experimental (full circles) and theoretical values of elastic parameters. In the figures eighter the conversion of epoxy groups, α_{E}, or parameter defining the strength of the substitution effect, ρ, varies at constant value of the other constituent. The arrow indicates increase of α_{E} (a) and ρ (b).

4.3.3 Thermal properties

DSC traces obtained for non-extracted and extracted networks in heating rate of 10 °C/min are shown in Figure 4.20 and Figure 4.21, respectively. Single glass transition is registered for all networks, the same trends as observed by DMA are confirmed. Crystallization or melting of ED600 or PDGEBA in the networks is not observed since it is completely suppressed by crosslinking.

Values of the glass transition temperature and the change in the specific heat in glass transition were determined by the half step height method. These data are given in Table 4.3, the values of glass transition temperatures determined by DMA at frequency f=0.1 Hz are included for comparison. They exhibit the same trend as the data determined by DMA.

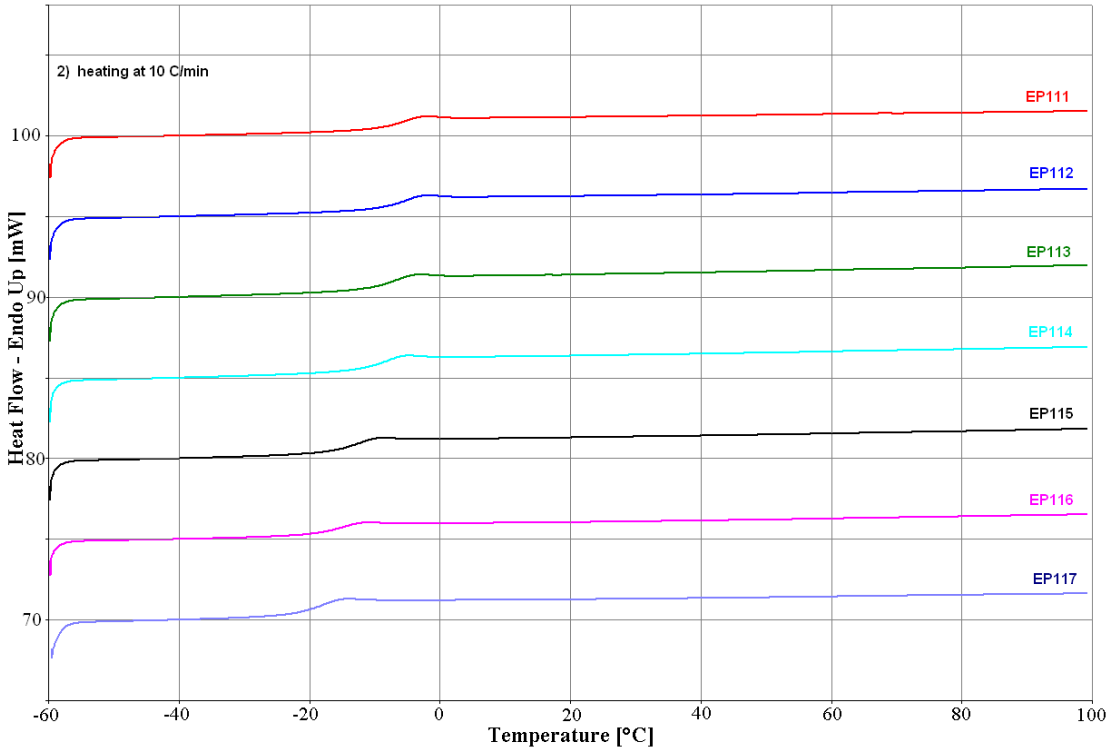

Figure 4.20: DSC thermograms of non-extracted networks determined in heating at 10 °C/min. Each spectrum has been shifted vertically for clarity of the presentation.

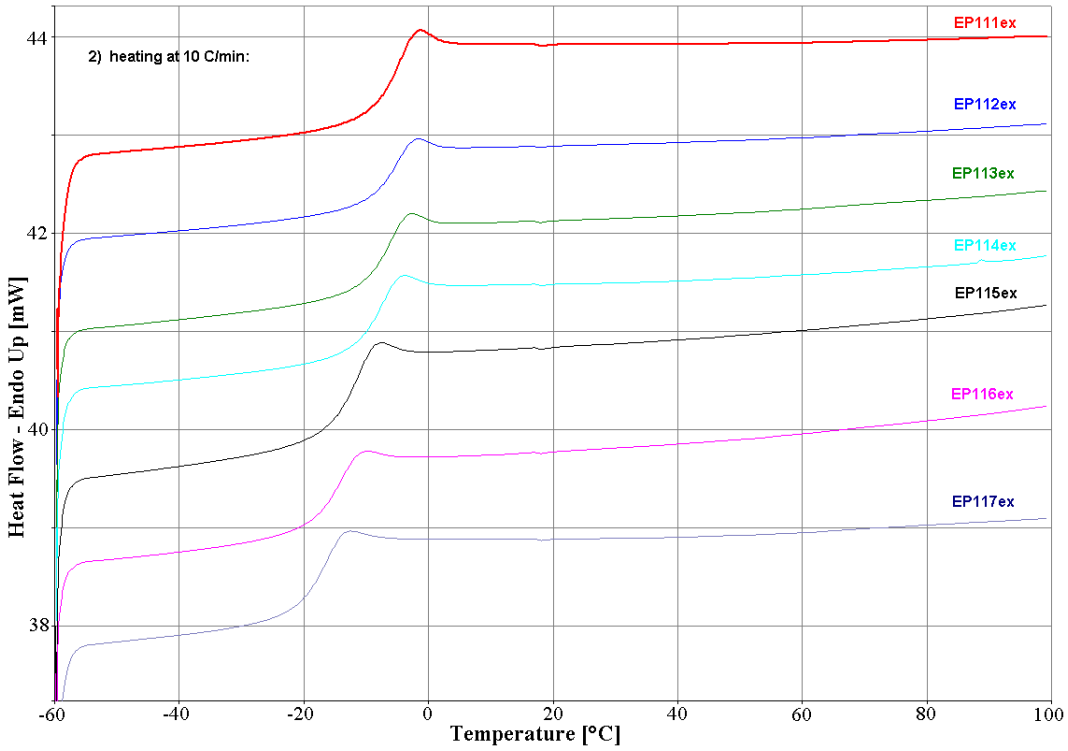

Figure 4.21: DSC thermograms for extracted networks determined in heating at 10 °C/min. Each spectrum has been shifted vertically for clarity of the presentation.

r	T_α, DMA – 0.1 Hz [°C]		T_g, DSC [°C]		Δc_p, DSC [$Jg^{-1}K^{-1}$]	
	non-ext.	extracted	non-ext.	extracted	non-ext.	extracted
2.00	-19.3	-16.8	-19.2	-17.6	0.599	0.548
1.75	not measured	not measured	-15.9	-15.3	0.524	0.512
1.50	-12.5	-10.4	-13.6	-12.4	0.521	0.509
1.25	-8.0	-7.8	-9.5	-8.9	0.517	0.493
1.12	-6.0	-6.6	-8.2	-7.6	0.507	0.478
1.06	-5.5	-5.5	-6.7	-6.3	0.475	0.474
1.00	-4.0	-4.0	-6.5	-5.9	0.448	0.455

Table 4.3: The glass transition temperatures of samples as result of various methods (DMA and DSC) and difference of heat capacity obtained by DSC.

To conclude, DMA and DSC experiments give no evidence for a phase separation in the epoxy networks prepared.

4.4 Epoxy hydrogels

4.4.1 Swelling

Swelling of epoxy networks in various solvents has been investigated. Volume fraction of polymer network in hydrogel was calculated from the mass increase due to water absorption assuming additivity of volumes as

$$v_p = \frac{1}{1 + \left(\frac{m}{m_\mathrm{p}} - 1\right)\frac{d_\mathrm{s}}{d_\mathrm{p}}} \tag{4.1}$$

where m and m_p are the masses of the hydrogel and dry extracted network, d_s and d_p are the specific masses of solvent and dry extracted network, respectively. Volume fraction of the solvent is simply: $v_\mathrm{s} = 1 - v_\mathrm{p}$.

Figure 4.22 shows a comparison of the swelling behaviour of epoxy networks. The strongest change of the swelling degree of the networks with stoichiometric ratio was found for water. This is from two reasons. Firstly, the concentration of elastically active junctions decreases with increasing r (the network is more compliant). Secondly, the content of hydrophilic component (POE) increases with r, see Table 3.1. Other solvents are good solvents for all the network components (POE, POP and PDGEBA) and the swelling trend is not so steep, especially, for benzene and toluene.

4.4.2 Structure by SANS

SANS patterns obtained for the gels prepared by swelling of the networks in deuterated methanol are shown in Figure 4.23. Scattering intensity is monotonously decaying with magnitude of scattering vector. This behaviour is typical for the networks swollen in good solvent, see Chapter 1. In this case, the scattering intensity is governed by frozen and dynamic inhomogeneities, only, which are caused by inhomogeneous space distribution of network junctions and thermal movement of polymer network chains and solvent molecules, respectively [30]. The scattering data can be fitted by eq. 1.7.

Figure 4.24 illustrates the difference in SANS behavior when the same networks are swollen in deuterated water. Scattering peak is presented in all scattering patterns except for the hydrogels swollen to highest degrees (the networks EP116 and 117). As a parameter giving an estimation of the length scale of inhomogeneous structure, the Bragg distance, D_B, can be used. It is related to the position of the scattering peak, q_max, by $D_\mathrm{B} = 2\pi/q_\mathrm{max}$. For the hydrogels prepared from EP111 - 115, D_B obtains values between 70 and 100 Å. It can be concluded that the hydrogels have nanophase separated structure. Hydrogels swollen to highest degrees (EP 116 and 117) show very strong monotonously decaying scattering, however, these scattering data cannot be fitted to eq. 1.7.

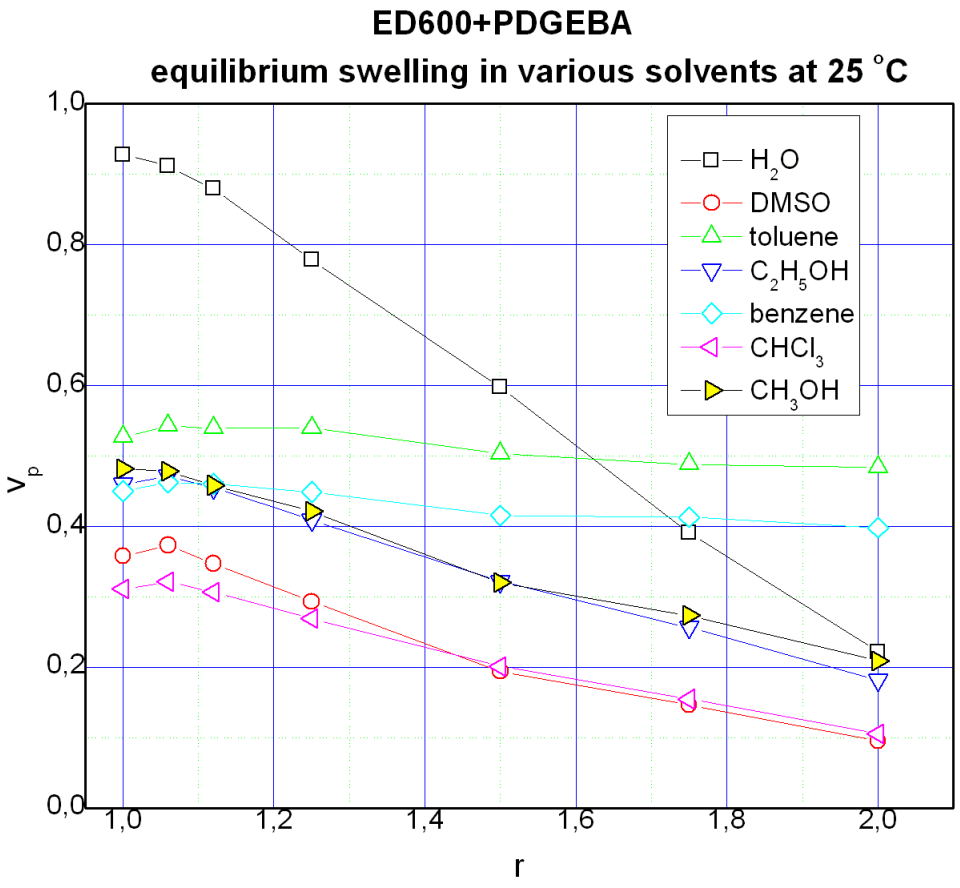

Figure 4.22: Swelling of the networks in various solvents at 25 °C. v_p denotes the volume fraction of polymer network in the swollen state, r is the stoichiometric ratio.

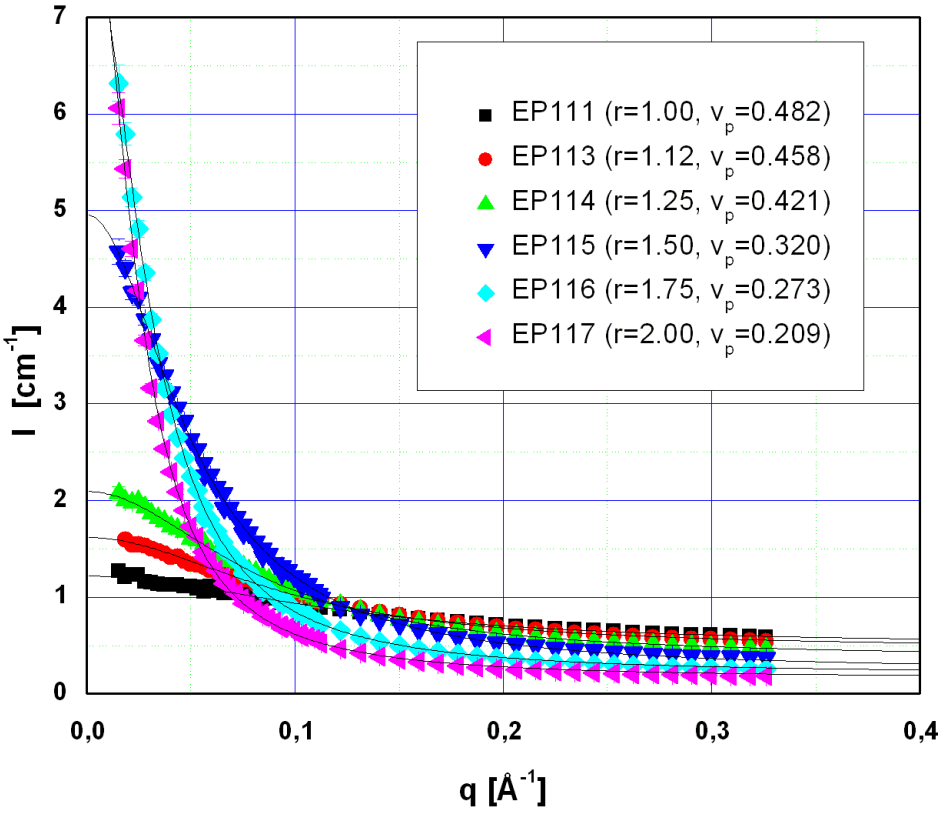

Figure 4.23: SANS patterns of the gels prepared by swelling of epoxy networks in CD_3OD to equilibrium at 25 °C. Solid lines represent fits according to eq. 1.7, v_p denotes the volume fraction of polymer network in the swollen state.

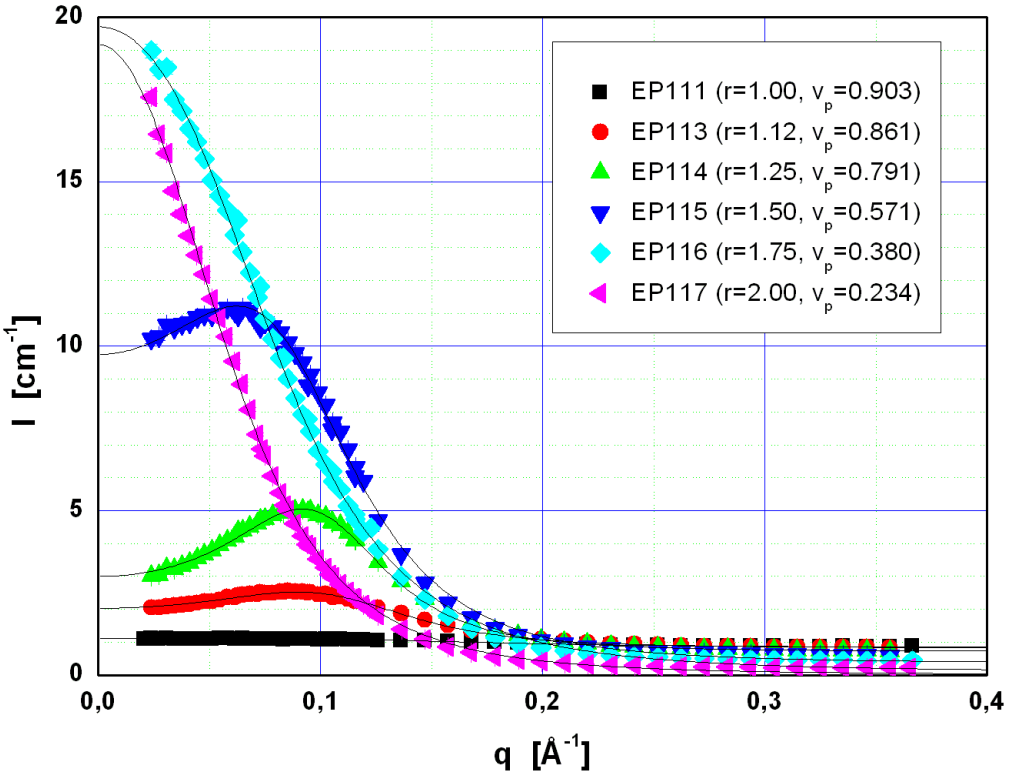

Figure 4.24: SANS scattering profile of all the studied hydrogels swollen in D_2O to equilibrium at 25 °C. Solid lines represent fits according to Teubner-Strey model, see eq.1.11.v_p denotes the volume fraction of polymer network in the swollen state.

Sample in CD_3OD	I_B [cm^{-1}]	$\frac{kT\nu_p(\rho_s-\rho_p)^2}{M_{osm}}$ [cm^{-1}]	ξ_L [$\AA$]
EP 111	0.504	0.717	8.0
EP 113	0.462	1.160	10.3
EP 114	0.367	1.733	12.1
EP 115	0.234	4.740	19.6
EP 116	0.204	7.711	33.1
EP 117	0.161	8.337	41.6

Table 4.4: Parameters obtained by fitting of SANS data shown in Fig. 4.23 to eq. 1.7.

Analysis of the SANS patterns shown in Figure 4.24 in the descending region of the scattering intensity reveals that coherent part of the scattering intensity (i.e., after subtraction the incoherent scattering background, I_B assumed to be constant) decays for all samples as q^{-n} with $n \approx 3-5$. This value is much higher than value expected for the polymer networks swollen in good solvent ($n < 2$, see eq. 1.7). Therefore, similarly to the previous system reported in [19], a kind of phase separated structure consisting of domains rich and poor in D_2O is expected for all hydrogels. To get more detailed information from the SANS data about the structure of the hydrogels a proper model providing a formula for the scattering intensity in terms of some structural parameters is needed. First, the Percus–Yevick model used successfully in SANS investigation of a similar system with longer POE block (see section 1.5.3) was tried. However, it turned out that for the systems discussed here, the Percus–Yevick model fails.

Therefore, an attempt to find another model for fitting scattering patterns was made. Model developed by Teubner and Strey [31], described in chapter 1, proved very well to this purpose.

Scattering curves obtained by fitting experimental data to Teubner–Strey formula are also shown in Figure 4.24. The fits are very good and the values of three fitting parameters determined, the periodicity, D, persistence length, ζ, and mean square fluctuation of neutron scattering length, $\langle(\Delta\varrho)^2\rangle$), are given in Table 4.5.

Except for the hydrogel swollen to highest degree, the mean square fluctuation of the scattering length density grows with increasing stoichiometric ratio r of the epoxy networks used in swelling. Similarly, the periodicity D, increases from the value of about 47 Å for the hydrogel obtained by swelling of stoichiometric network to 233 Å for the hydrogel with highest swelling degree. Unlike this, a different dependence is found for the persistence length, ζ. This parameter grows initially from the value of ca 8 Å in the hydrogel prepared by swelling of stoichiometric network to 23 Å for the hydrogel made from EP 114 ($r = 1.25$). Then it decreases again to a value about 12 Å for hydrogel prepared by swelling of the network EP 117 ($r = 2.00$).

The values of $\langle(\Delta\varrho)^2\rangle$ are also given in Table 4.5 and can be compared with the values which may be expected from a two-density model of the phase separated structure. In the case of sharp boundaries between phases

Sample in D_2O (ex)	model 1 $\lvert\varrho_A - \varrho_B\rvert$ $[10^{10}cm^{-2}]$	model 1 $\langle(\Delta\varrho)^2\rangle$ $[10^{20}cm^{-4}]$	model 2 $\lvert\varrho_A - \varrho_B\rvert$ $[10^{10}cm^{-2}]$	model 2 $\langle(\Delta\varrho)^2\rangle$ $[10^{20}cm^{-4}]$	experiment $\langle(\Delta\varrho)^2\rangle$ $[10^{10}cm^{-2}]$	D [Å]	ζ [Å]
EP 111	5.39	2.56	1.79	0.61	0.87	47	8
EP 112	5.40	2.32	1.59	0.47	0.93	49	9
EP 113	5.41	3.49	2.26	1.07	1.90	58	17
EP 114	5.42	4.86	2.88	1.92	3.27	61	23
EP 115	5.45	7.26	4.06	4.07	7.51	73	17
EP 116	5.46	7.02	4.66	4.46	7.98	114	13
EP 117	5.47	5.37	4.99	3.61	4.86	223	12

Table 4.5: Parameters of the hydrogel structure calculated for two two-phase models and those determined by fitting SANS data to eq.1.11. Model 1: phase A = D_2O, phase B = POE + POP + PDGEBA. Model 2: phase A = D_2O +POE, phase B = POP + PDGEBA.

$$\langle(\Delta\varrho)^2\rangle = v_A v_B(\varrho_A - \varrho_B)^2 \tag{4.2}$$

where v_A and v_B are the volume fractions, ϱ_A and ϱ_B are the scattering length densities of the phases A and B.

The scattering length density of a phase can be calculated by suming contributions from all nuclei contained in the phase of the volume V as

$$\varrho = \frac{\sum_i b_i}{V} \tag{4.3}$$

where b_i is the coherent scattering length of the nucleus i.

No assumption about the morphology of the system is needed in eq. 4.2. In Table 4.5, there are given the values of $\langle(\Delta\varrho)^2\rangle$ expected for two alternatives. In the first case, it is assumed that the phases consist of D_2O and organic components (POE, POP and PDGEBA), respectively – model 1. In the second case, the phases consist of the mixture of the POE blocks from ED600 with D_2O and the mixture of the hydrophobic components (POP and PDGEBA), respectively – model 2. The values of the volume fractions of the phases for both models were calculated using data given in Table 4.5 assuming additivity of volumes. Neutron scattering length densities of the phases in the models were calculated as the volume averages of the neutron scattering length densities of their constituents. Values of the specific mass, d, and the neutron scattering length density of the constituents, ϱ, are given in 4.6. From the results, it can be seen that for most hydrogels, the values of $\langle(\Delta\varrho)^2\rangle$ determined from fitting of experimental data are between the values given by above two cases.

Before interpretation of the origin of the difference in the structure of gels prepared by swelling epoxy networks in methanol and water as revealed by SANS it will be useful to recall topology of the epoxy networks. Formation of long sequences of diepoxide (PDGEBA) units is one of the characteristic features of the reaction

Component	d [g cm^{-3}]	ϱ [10^{10} cm^{-2}]
POE	1.08	0.61
POP	1.01	0.35
PDGEBA	1.09	1.15
D2O	1.10	6.34

Table 4.6: Specific masses, d, and coherent neutron scattering length densities, ϱ, of the components at 25 °C

between diamine and diepoxide (see Figure 4.25). In our system, the PDGEBA chains are incorporated into network structure by ED600 chains that are grafted to them. In a perfect stoichiometric epoxy network a single long PDGEBA chain would be intervowen (see Figure 4.25a). With deviation from stoichiometric network (for $r > 1$), PDGEBA content becomes smaller and the single PDGEBA chain is split into a distribution of shorter chains whose average length decreases with increasing stoichiometric ratio. The PDGEBA chains remain interconnected by ED600 chains to the network structure, however, pending ED600 chains linked to the network by one terminal, only, appear in the system (see Figure 4.25b). The number of pending ED600 chains grows with increasing r and this topological restriction becomes weaker until it extincts at the gel-point.

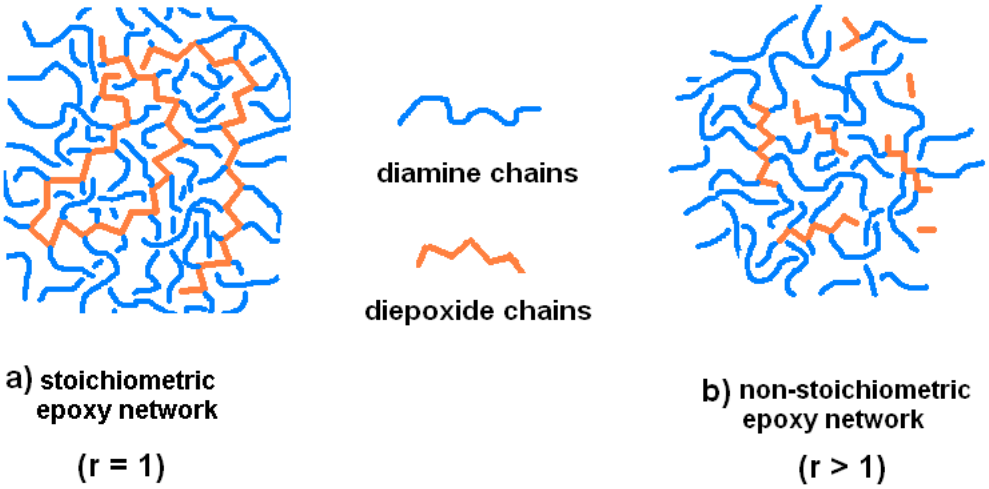

Figure 4.25: Comparison of topologies of stoichiometric (a) and non-stoichiometric (b) epoxy network.

When a solvent is absorbed by the network and the volume of the system increases, topology of the network has to be conserved. As regards the hydrogel structure, depending on the interaction of polymer network chains with solvent two situations are possible. First situation occurs when mixing of all chains with the solvent is thermodynamically favorable and there is not a tendency to phase separation of some

chains. This occurs in epoxy networks swollen in methanol. The composition and density fluctuations in the system are governed by thermal motion of the polymer chains and solvent molecules respecting the network topology. Another contribution from inhomogenous space distribution of network junctions can be also found in low q-region of SANS patterns. However, if the network consists of chains significantly differing in interaction with the solvent, in the swelling process the chains tend to phase separate to solvent-rich and solvent-poor regions. The phase separation cannot evolve to a macroscopic length scale and it is shortened to a size respecting conservation of network topology, i.e. nanometer scale. This is the case of epoxy hydrogels prepared by swelling of epoxy networks in water. The thermodynamic incompatibility of one of the part of the system with water force the hydrophilic and hydrophobic components, respectively, to form locally parallel arrangement of domains described by the Teubner-Strey model.

4.4.3 Mechanical properties

Stress-strain curves were obtained by stretching of hydrogel strips immersed in water. The measurements were performed at constant force rate 40 mN/min. Values of Young modulus were determined from the initial slope of a few stress-strain cycles as averages over five values. Typical stress-strain curve is shown in Figure 4.26.

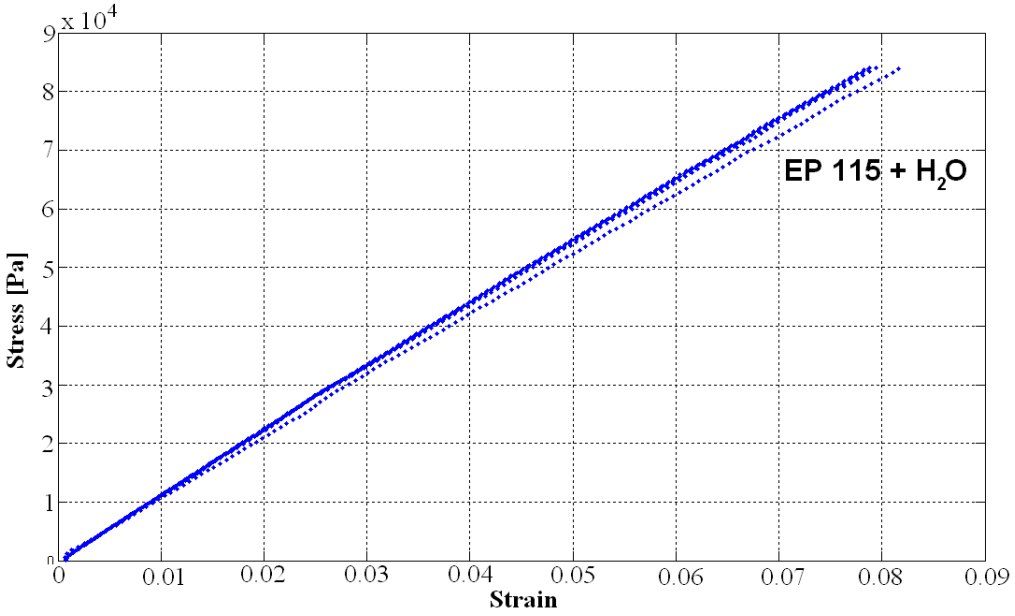

Figure 4.26: Stress-strain behaviour of hydrogel prepared from the network EP115

For comparison, dry non-extracted networks were also measured in the same way. Values of moduli determined for both systems are given in Table 4.7, together with the values obtained from dynamical experiment for non-extracted samples.

Surprisingly, for almost all hydrogels the values of Young modulus are close or even higher than those determined for dry non-extracted networks. The only exception is the hydrogel with highest content of water (EP117). Modulus of dry networks

Sample	r	v_p	E_{dyn} [MPa]	E_{netw} [MPa]	E_{hgel} [MPa]
EP111	1.00	0.928	2.45	2.28	2.48
EP112	1.06	0.911	2.23	2.70	2.67
EP113	1.12	0.880	3.46	2.41	2.63
EP114	1.25	0.778	2.44	1.82	1.98
EP115	1.50	0.597	0.94	1.11	1.11
EP116	1.75	0.391	not measured	0.63	0.65
EP117	2.00	0.222	0.60	0.41	0.29

Table 4.7: Mechanical properties of the non-extracted networks and hydrogels determined from stress-strain curves at 20 °C: E_{netw} and E_{hgel} denote Young moduli of non-extracted network and hydrogel, respectively, E_{dyn} is elastic modulus of non-extracted networks obtained by dynamical experiment at 0.1 Hz and 20 °C. r is the stoichiometric ratio and v_p is the volume fraction of the polymer network in swollen state.

obtained by dynamical experiment is much higher for the sample EP 113 which is caused by interruption of experiment at this temperature region. The temperature inside the sample should differ from that measured by the device near the sample.

4.4.4 Thermal properties

In DSC experiments, small specimen cut from hydrogels were closed in aluminium sample pans, cooled down from 30 °C to -53 °C at cooling rate 10 °C/min, equilibrated at this temperature for 5 min and heated again to 50 °C at 10 °C/min.

Figure 4.27 shows DSC thermograms obtained in cooling. For hydrogels with lower content of water (from EP111-EP114), only glass transition of the hydrogel is observed (at ca -30 °C)[2]. When the amount of water is higher (in EP115 hydrogel), crystallization of water appears first (at ca -10 °C) followed by glass transition of the network swollen with water. Increasing further the content of water a peak due to crystallization of undercooled water appears at ca -11 °C. Finally, another crystallization peak is observed when content of water is even higher. The position of the last peak is very sensitive to the content of water and can be attributed to the fraction of water strongly interacting with POE.

Figure 4.27 shows DSC thermograms obtained in heating. For hydrogels with lower content of water (from EP111-EP113), only glass transition of the hydrogel is observed again (values are given in Table 4.8). For somewhat higher amount of water(in hydrogel EP114) recrystallization and melting of water is found around 0 °C. In hydrogels with even higher content of water, this peak grows and is preceded by peak from the water strongly interacting with POE.

Some parameters determined from DSC are given in Table 4.8.

[2]a small peak at ca -42 °C presented in the insert of Fig. 4.27 as well as a sudden change of the DSC traces at lower temperatures is caused by the cooling system (INTRACOOLER I) which is not able to control cooling at temperatures lower than -40 °C.

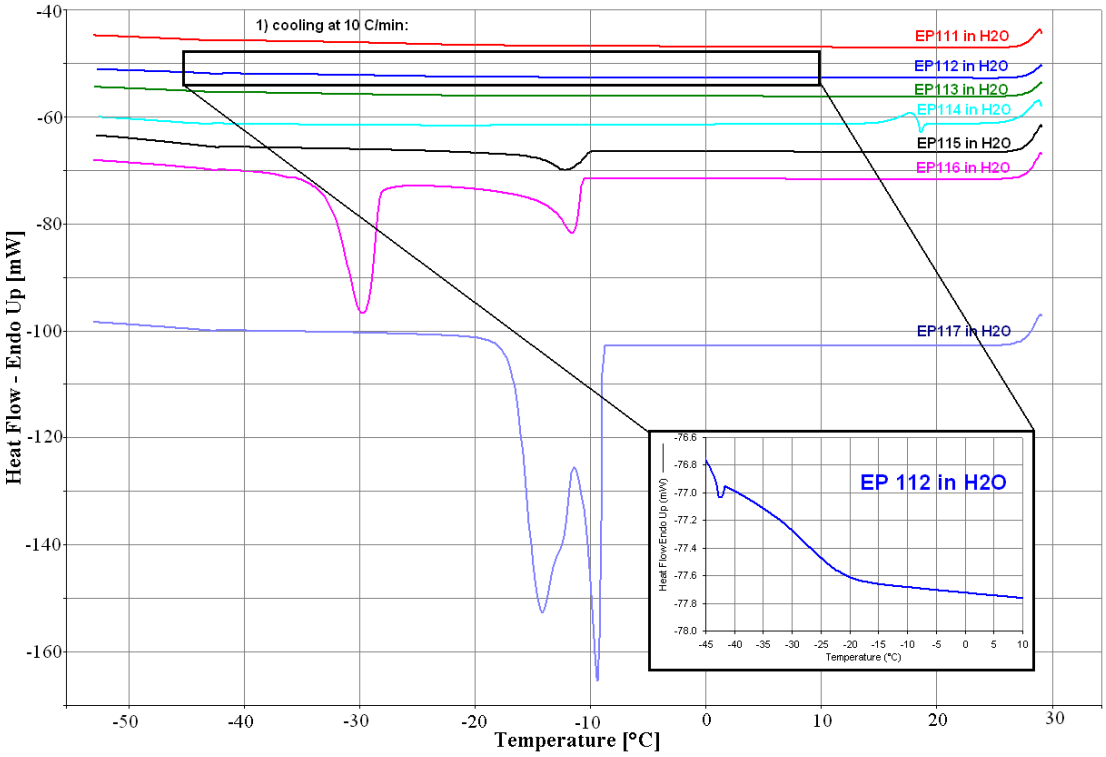

Figure 4.27: DSC thermograms obtained for the networks swollen in H_2O in cooling at 10 °C/min. The curves are vertically shifted for clarity. The insert shows a detail of the glass transition region for one of the hydrogels with lower content of water (EP112 hydrogel).

Sample in H_2O	r	v_p	ΔH_{c1} [Jg^{-1}]	ΔH_{c2} [Jg^{-1}]	ΔH_{m1} [Jg^{-1}]	ΔH_{m2} [Jg^{-1}]
EP111	1.00	0.928	—	—	—	—
EP112	1.06	0.911	—	—	—	—
EP113	1.12	0.880	—	—	—	—
EP114	1.25	0.778	—	1.0	—	-1.0
EP115	1.50	0.597	—	10.2	-24.5	-351
EP116	1.75	0.391	54.2	29.2	-10.5	-122
EP117	2.00	0.222	129.0	65.0	—	-206

Sample in H_2O	r	v_p	T_{g1} [°C]	Δc_{p1} [$Jg^{-1}K^{-1}$]	T_{g2} [°C]	Δc_{p2} [$Jg^{-1}K^{-1}$]
EP111	1.00	0.928	-22.4	0.447	34.6	0.114
EP112	1.06	0.911	-23.8	0.439	34.1	0.150
EP113	1.12	0.880	-26.2	0.375	34.7	0.100
EP114	1.25	0.778	-31.9	0.196	—	—
EP115	1.50	0.597	—	—	—	—
EP116	1.75	0.391	—	—	—	—
EP117	2.00	0.222	—	—	—	—

Table 4.8: DSC parameters dependent on ratio of monomers r determined for the hydrogels prepared by swelling of epoxy networks in H_2O. v_p denotes volume fraction of polymer, ΔH_{c1}, ΔH_{c2} are enthalpy increments of crystallization, ΔH_{m1}, ΔH_{m2} are enthalpy increments of melting, T_{g1} and T_{g2} are the first and second glass transition temperatures, Δc_{p1} and Δc_{p2} mean change of molar thermal capacity at constant pressure determined from both glass transitions if any.

Closer look at DSC thermograms from heating reveals interesting feature in hydrogels with lower content of water (from EP111-114), see Figure 4.29. At ca 34 °C, another glass transition appears. It becomes less distinct with increasing content of water and absent in thermograms for with higher amount water (from EP115-117). This transition can be attributed to the glass transition of water-poor phase concluded from SANS measurements on hydrogels. The presence of this phase which is in glassy state at room temperature, causes that the values of Young modulus determined for hydrogels with intermediate content of water are unexpectedly high. However, to confirm this idea more experiments (e.g. temperature dependence of stress-strain measurements of hydrogels) are necessary.

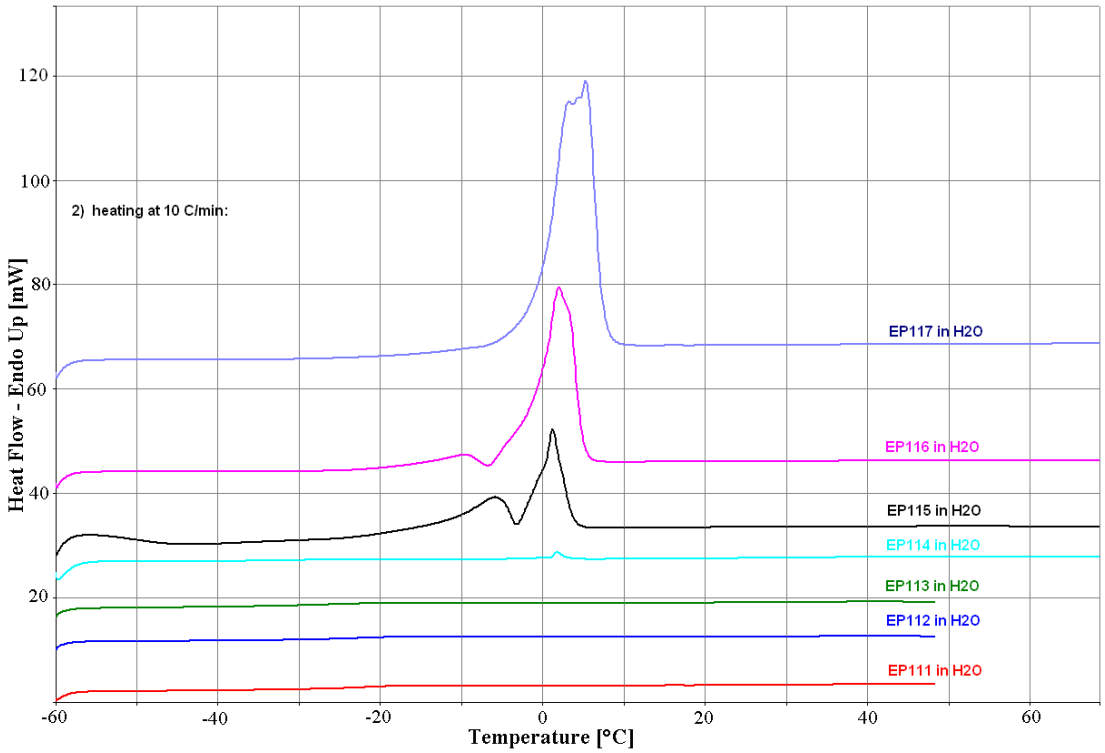

Figure 4.28: DSC thermograms obtained for the networks swollen in H_2O in heating at 10 °C/min. The curves are vertically shifted for clarity.

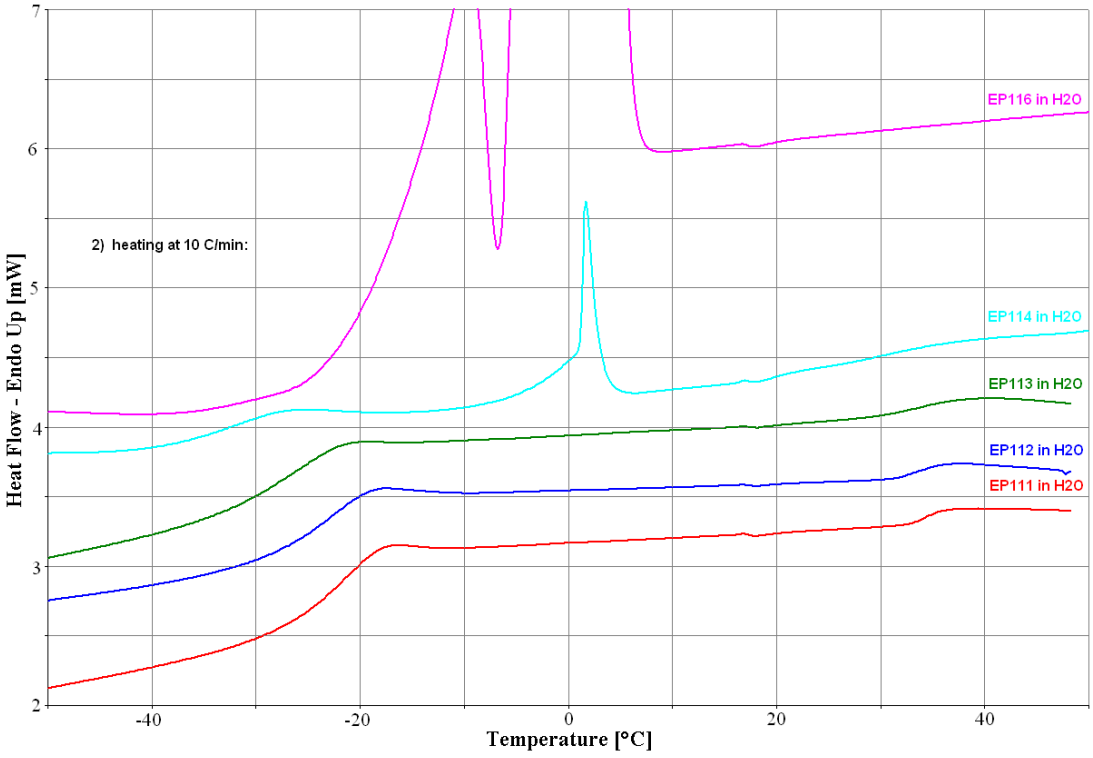

Figure 4.29: Details of DSC thermograms of the hydrogels prepared from EP111-114 and EP116 shown in Figure 4.28. The thermograms are shifted vertically.

Chapter 5

Conclusions

- Series of hydrophilic epoxy networks was prepared by reaction of α,ω- diamino terminated poly(oxypropylene)-*b*-poly(oxyethylene)-*b*-poly(oxypropylene) with Bisphenol A propoxylate diglycidyl ether at various values of initial ratio of amino and epoxy groups.

- Study of network formation for stoichiometric mixture (r=1) confirmed a decrease of reactivity of hydrogens in the secondary amines formed in the process relative to hydrogens in primary amines (substitution effect). This decrease is reflected in population of reaction products as detected by GPC and FTIR. Conversion of epoxy groups in gel point obtains value higher than that predicted for random reaction.

- Both, DMA and DSC, give no evidence about a phase separation in the epoxy networks prepared.

- Mechanical properties of the networks in rubbery state correspond to the conversion of epoxy groups, $\alpha \approx 0.90$.

- Series of epoxy hydrogels was prepared by swelling of the epoxy networks in D_2O and investigated by SANS. Amount of D_2O absorbed in hydrogels is controlled by the content of the hydrophilic component (POE) and cross-linking degree of the networks, both being functions of their composition described by the stoichiometric ratio.

- Nanophase separated structure in all hydrogels was revealed by SANS. Unlike a similar system prepared previously using longer POE block in the diamine different kind of the structure was found by SANS. Percus-Yevick model used in the previous system fails in fitting the SANS data from the present system. However, the SANS data are fitted very well to the Teubner-Strey model assuming locally lamellar order in the hydroegls.

- Formation of this order can be attributed to the conservation of polymer network topology and shorter length (lower content) of hydrophilic blocks (POE) in the epoxy networks.

Appendix A

Epoxy network parameters by theory of branching processes

For the convenience of the reader, in this appendix the most important formulas from theory of branching processes as applied to epoxy curing are given. This part is based mainly on paper by Dušek [11].

In the theory of branching processes, the structure of epoxy network in some reaction time (or extent of reaction) is "reconstructed" stochastically using diamine and diepoxide units. Structural parameters of epoxy network can be calculated by virtue of initial composition of the system and distribution of diamine and diepoxide units. Composition of reaction system is usually expressed using stoichiometric ratio, r defined by

$$r = \frac{2[\mathrm{NH_2}]_0}{[\mathrm{E}]_0} \tag{A.1}$$

where $[\mathrm{NH_2}]_0$ and $[\mathrm{E}]_0$ are initialmolar concentrations of amino and epoxy groups, respectively.

Molar and weight fractions of diamine and diepoxide units in the system are related to the stoichiometric ratio by:

$$n_1 = \frac{r}{r+2} \tag{A.2}$$

$$n_2 = 1 - n_2 \tag{A.3}$$

and

$$w_1 = \frac{M_1 r}{M_1 r + 2M_2} \tag{A.4}$$

$$w_2 = 1 - w_2 \tag{A.5}$$

where M_1 (M_2) is the molar masses of diamine (diepoxide).

Apportionment of building blocks from diamines an diepoxides are classified according to numbers of unreacted (hydrogen or epoxy) groups i, bonds with finite (j) and infinite (k) continuation , p_{ijk} and q_{ijk}. They are listed in Fig. A.1.

The key parameters in calculation of epoxy network structure are extinction probabilities of bonds originating from diamine and diepoxide, $v_{\mathrm{A}}, v_{\mathrm{E}}$. They are solutions of the nonlinear system of equations (eq.A.6) from the interval $< 0, 1 >$.:

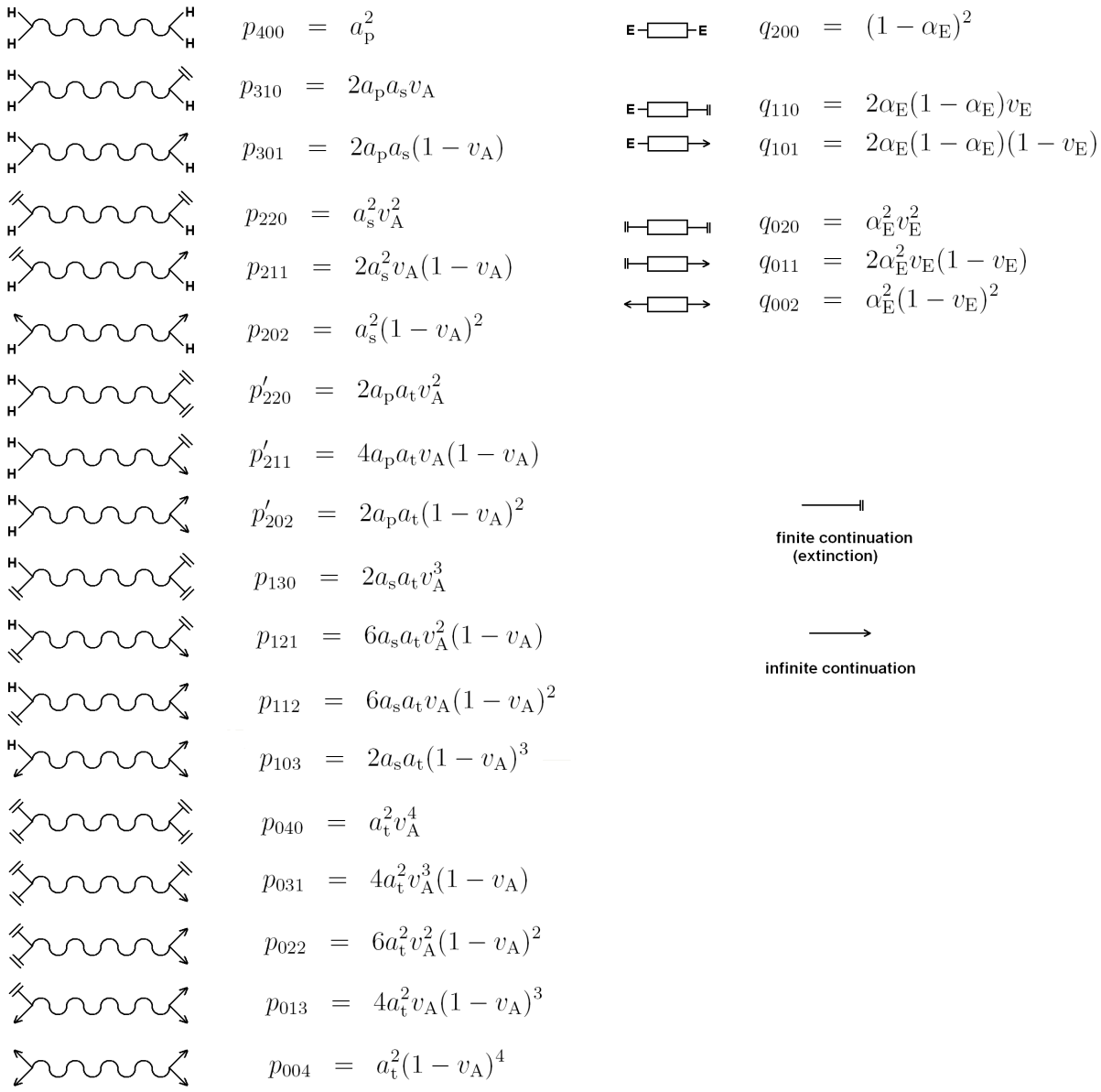

Figure A.1: Apportionments of building blocks from diamine (p_{ijk}) and diepoxide (q_{ijk}) for reconstruction of epoxy network by theory of branching processes. Molar fractions of primary, secondary and tertiary amino groups are denoted by $a_\mathrm{p}, a_\mathrm{s}, a_\mathrm{t}$, respectively. Conversion of epoxy groups is α_E, extinction probabilities of bonds originating from diamine and diepoxide are v_A and v_E, respectively.

$$v_{\mathrm{A}} = \frac{(a_{\mathrm{p}} + a_{\mathrm{s}} v_{\mathrm{E}} + a_{\mathrm{t}} v_{\mathrm{E}}^2)(a_{\mathrm{s}} + 2a_{\mathrm{t}} v_{\mathrm{E}})}{a_{\mathrm{s}} + 2a_{\mathrm{t}}} \tag{A.6}$$

$$v_{\mathrm{E}} = 1 - \alpha_{\mathrm{E}} + \alpha_{\mathrm{E}} v_{\mathrm{A}} \tag{A.7}$$

where $a_{\mathrm{p}}, a_{\mathrm{s}}, a_{\mathrm{t}}$ denote the molar fractions of primary, secondary and tertiary amino groups and α_{E} is the conversion of epoxy groups.

As dictated by the equations of chemical kinetics of epoxy resins curing the molar fractions of secondary and tertiary amino groups can be expressed by virtue of the molar fraction of primary amino groups as

$$a_{\mathrm{s}} = \frac{1}{1-\rho}\left(a_{\mathrm{p}}^{\rho} - a_{\mathrm{p}}\right) \tag{A.8}$$

$$a_{\mathrm{p}} = 1 - \frac{\rho}{1-\rho}\left(\frac{a_{\mathrm{p}}^{\rho}}{\rho} - a_{\mathrm{p}}\right) \tag{A.9}$$

where unequal reactivity of hydrogens from secondary and primary hydrogens (substitution effect) is taken into account. Parameter ρ is a measure of the strength substitution effect, it obtains values $\rho = 1/2$ for equal reactivity of all hydrogens, $\rho < 1/2$ when hydrogens from secondary amino groups are less reactive. Epoxy groups in diepoxide are usually separated by sequence of many atoms and, consequently, independent reactivity is assumed. For details, see [11] and references within.

Total conversion of amino groups is

$$\alpha_{\mathrm{A}} = a_{\mathrm{s}} + 2a_{\mathrm{t}} \tag{A.10}$$

and is related to the conversion of epoxy groups, α_{E} by

$$\alpha_{\mathrm{E}} = r\alpha_{\mathrm{A}} \tag{A.11}$$

The mass fractions of units contained in sol, w_{S}, dangling chains, w_{DC} and elastically active network chains, w_{EANC}, respectively, are given by

$$\begin{aligned} w_{\mathrm{S}} &= w_1(p_{400} + p_{310} + p_{220} + p'_{220} + p_{130} + p_{040}) \\ &+ w_2(q_{200} + q_{110} + q_{020}) \end{aligned} \tag{A.12}$$

$$w_{\mathrm{DC}} = w_1(p_{301} + p_{211} + p'_{211} + p_{121} + p_{031}) + w_2(q_{101} + q_{011}) \tag{A.13}$$

$$w_{\mathrm{EANC}} = 1 - w_{\mathrm{S}} - w_{\mathrm{DC}} \tag{A.14}$$

For numbers of elastically active junctions per one molecule of initial reaction system, μ_{a}/N and chains, ν_{a}/N, respectively, for rigid diamine units one gets

$$\frac{\mu_{\mathrm{a}}}{N} = n_1(p_{103} + p_{013} + p_{004}) \tag{A.15}$$

$$\frac{\nu_{\mathrm{a}}}{N} = \frac{1}{2}\left[3n_1(p_{103} + p_{013}) + 4n_1 p_{004}\right] \tag{A.16}$$

Similarly for elastic diamine units one obtains

$$\frac{\mu_{\mathrm{a}}}{N} = n_1(p_{103} + p_{013} + 2p_{004}) \tag{A.17}$$

$$\frac{\nu_{\mathrm{a}}}{N} = \frac{1}{2}\left[3n_1(p_{103} + p_{013}) + 6n_1 p_{004}\right] \tag{A.18}$$

Cycle rank per one molecule of initial reaction system, ξ/N, is the difference between numbers of elastically active chains and junctions:

$$\frac{\xi}{N} = \frac{\mu_{\mathrm{a}}}{N} - \frac{\nu_{\mathrm{a}}}{N} \tag{A.19}$$

and does not depend on rigidity of diamine units.

Number of elastically active chains and cycle rank, respectively, are related to Young modulus of affine and phantom network by eq. 1.20 and 1.21. For epoxy networks, these quantities can be expressed by virtue of eq. A.16 and A.19 and specific mass of the network as

$$E_{\mathrm{aff}} = \frac{3}{2} dRT \frac{\nu_{\mathrm{a}}}{N}(w_1 c_{\mathrm{A}} + w_2 c_{\mathrm{E}}) \tag{A.20}$$

$$E_{\mathrm{ph}} = \frac{3}{2} dRT \frac{\xi}{N}(w_1 c_{\mathrm{A}} + w_2 c_{\mathrm{E}}) \tag{A.21}$$

To eliminate the dependence on specific mass of the networks, d, reduced Young modulus, E_{red}, defined as

$$E_{\mathrm{red}} = \frac{E}{3dRT} \tag{A.22}$$

is introduced for comparison of theoretical and experimental values. Thus, reduced modulus of affine and phantom network is:

$$E_{\mathrm{red}}^{\mathrm{aff}} = \frac{1}{2}\frac{\nu_{\mathrm{a}}}{N}(w_1 c_{\mathrm{A}} + w_2 c_{\mathrm{E}}) \tag{A.23}$$

and

$$E_{\mathrm{red}}^{\mathrm{ph}} = \frac{1}{2}\frac{\xi}{N}(w_1 c_{\mathrm{A}} + w_2 c_{\mathrm{E}}) \tag{A.24}$$

Bibliography

[1] Krakovský, I.; Hanuš, J.; Pleštil, J.; Baldrin, J.; Salmerón Sánchez, M. *Structure and swelling behaviour of epoxy networks based on α, ω - diamino terminated poly(oxypropylene) – block – poly (oxyethylene) – block –poly (oxypropylene).* Polymer. 2005, 46, s. 109 – 119.

[2] Meloun, J.; Krakovský, I.; Nedbal, J.; Ilavský, M. *Effect of chemical clusters on photoelastic behaviour and small – angle X – ray scattering of epoxide networks based on poly(oxypropylene)diamines.* European Polymer Journal. 2000, 36, s. 2327 – 2335.

[3] Gómez Ribelles, J. L.; Salmerón Sanchez, M.; Torres de la Osa, L.; Krakovský, I. *Thermal transitions in α, ω - diamino terminated poly(oxypropylene) – block – poly (oxyethylene) – block –poly (oxypropylene) aqueous solutions and their epoxy networks.* Journal of Non – Crystalline Solids. 2005, 351, s. 1254 – 1260.

[4] Meissner, B.; Zilvar, V. *Fyzika polymerů* Praha: SNTL. 1987, s. 30 - 32.

[5] Green, M. M.; Wittcoff, H. A. *Organic chemistry principles and industrial practice.* Weinheim: WILEY – VCH Verlag, 2003.

[6] Mark, J. E.; Erman, B. *Rubberlike elasticity a molecular primer.* Canada: John Wiley and Sons, Inc., 1988.

[7] Clayten, A. M.*Epoxy resins: Chemistry and technology.* New York: MARCEL DEKKER, Inc., 1988.

[8] Adamson, A. W.; Gast A. P. *Physical Chemistry of Surfaces.* Canada: John Wiley and Sons, Inc., 1995.

[9] Tschoegl, N. W. *Fundamentals of equilibrium and steady - state thermodynamics* Netherlands: Elsevier Science. 2000, s. 126 - 128.

[10] Michalovic, M. *The Macrogalleria* [online]. 2005 [cit.2010-04-06]. Making Epoxy Resins. Available from WWW:⟨ http://www.pslc.ws/macrog.htm⟩.

[11] Dušek, K. *Network formation in curing of epoxy resins* Advances in Polymer Science. 1986, 78, 59 s.

[12] Sosnik, A.; Cohn, D. *Reverse thermo-responsive poly(ethylene oxide) and poly(propylene oxide) multiblock copolymers.* Biomaterials. 2005, 26, s. 349 – 357.

[13] Sosnik, A.; Cohn, D.*Ethoxysilane – capped PEO – PPO – PEO three-blocks: a new family of reverse thermo – responsive polymers.* Biomaterials. 2004, 25, s. 2851 – 2858.

[14] *Chemistry Homepage* [online]. 2007 [cit. 2010-04-07]. Gel Permeation Chromatography. Available from WWW: ⟨ http://academic.sun.ac.za/polymer⟩.

[15] *Microsoft Internet Information Server* [online]. 1996 [cit. 2010-04-06]. Equipment and Techniques. Available from WWW: ⟨ http://serwebdicma.ing.unibo.it/⟩.

[16] Borsali, R.; Pecora, R. *Soft-Matter Characterization* Berlin: Springer. 2008, s. 705 - 763.

[17] Shibayama, M.; et al. *Complementary use of small-angle neutron scattering and dynamic light scattering studies for structure analysis and dynamics of polymer gels.* Applied Crystallography. 2006, 40, s. 43 – 47.

[18] Laity, P. R.; et al. *A review of small-angle scattering models for random segmented poly(ether-urethane) copolymers.* Polymer. 2004, 45, s. 7273 – 7291.

[19] Krakovský, I.; Pleštil, J.; Almásy, L. *Structure and swelling behaviour of hydrophilic epoxy networks investigated by SANS.* Polymer. 2006, 47, s. 218 – 226.

[20] Krakovský, I.; Székely, N. *Small-angle neutron scattering study of nanophase separated epoxy hydrogels.* Journal of Non-cryst. Solids. 2010, 356, s. 368 - 373.

[21] *DMA 8000 : Dynamic Mechanical Analyzer.* USA : Perkin Elmer, 1998. 12 s. Available from WWW: ⟨ http://las.perkinelmer.com/⟩.

[22] Gedde, U. W. *Polymer Physics.* Netherlands: Springer. 1995, 298 s.

[23] Ferry, J. D. *Viscoelastic properties of polymers.* USA: John Wiley and Sons, Inc., 1980.

[24] James, H. M.; Guth, E. *Theory of the Elastic Properties of Rubber.* Journal of Chem. Physics. 1943, 11, s. 455 – 482.

[25] Wall, F. T.; Flory, P. J. *Statistical thermodynamics of rubber elasticity.* Journal of Chem. Physics. 1951, 19, s. 1435 –1439.

[26] Michalovic, M. *The Macrogalleria* [online]. 2005 [cit.2010-04-06]. Differential Scanning Calorimetry. Available from WWW: ⟨ http://www.pslc.ws/macrog.htm⟩.

[27] *Sigma-Aldrich* [online]. 2008 [cit. 2010-04-12]. Bisphenol A propoxylate diglycidyl ether. Available from WWW: ⟨http://www.sigmaaldrich.com⟩.

[28] Rosta, L. *Appl.Phys.* Physica A. 2002, 74, 52 s.

[29] Fernandez – Nograro, F.; Valea, A.; Llano – Ponte, R.; Mondragon, I. *Dynamic and mechanical properties of DGEBA/poly(oxypropylene) amine based epoxy resins as a function of stoichiometry.* Eur. Polym. J. 1996, 32, s. 257 – 266.

[30] Krakovský, I.; Székely, N.K. *SANS study of the structure of swollen copolymer networks* BNC, Exp. report. 2010.

[31] Székely, N.K.; Krakovský, I. *Dependence of nanophase separated structure of epoxy hydrogels on swelling conditions investigated by SANS.* European Polymer Journal. 2009, 45, s. 1385 – 1390.